Summer 2008

DEM simulated radial and axial pressure in a cylindrical granular column

Meng Cui
New Jersey Institute of Technology

ABSTRACT

DEM SIMULATED RADIAL AND AXIAL PRESSURE IN A CYLINDRICAL GRANULAR COLUMN

by
Meng Cui

The study of packed beds of granular spheres and their applications are of great interest to industries, and one of the most important subjects that has been studied is cylindrical beds. In 1895, H. A. Janssen discovered that in a vertical cylinder the pressure measured at the bottom does not depend upon the height of the filling in contrast to Newtonian fluids that possess linear hydrostatic pressure equilibrium. One of assumptions of his theory stated that the horizontal pressure is proportional to the vertical. In this thesis, this physical hypothesis is investigated using Discrete Element Simulations of inelastic with a cylindrical vessel and an axial pressure load. In addition, we studied the radial solid fraction to better understand the pattern of radial pressure evolution. The force model that corresponds to linear spring-dashpot model and energy dissipation is simulated by frictional forces: inter-particle and particle-wall. In this model, the frictional forces at the wall are activated by moving the piston floor downwards with small velocity. The diameter of the cylinder is set to 13.33 diameters of particle and the fill heights are in the range from 0.262 to 10.172. Results obtained in the simulations show the limits of Janssen's theory applicability within granular physical phenomenon, and also provide a strong foundation for further theoretical analysis.

DEM SIMULATED RADIAL AND AXIAL PRESSURE IN A CYLINDRICAL GRANULAR COLUMN

by
Meng Cui

A Thesis
Submitted to the Faculty of
New Jersey Institute of Technology
in Partial Fulfillment of the Requirements for the Degree of
Master of Science in Mechanical Engineering

Department of Mechanical Engineering

August 2008

APPROVAL PAGE

DEM SIMULATED RADIAL AND AXIAL PRESSURE IN A CYLINDRICAL GRANULAR COLUMN

Meng Cui

8-25-2008

Dr. Anthony Rosato, Thesis Advisor — Date
Professor of Mechanical Engineering, NJIT

7/21/08

Dr. Ian S. Fischer, Committee Member — Date
Professor of Mechanical Engineering, NJIT

8-20-2008

Dr. David J. Horntrop, Committee Member — Date
Associate Professor of Mathematical Sciences, NJIT

BIOGRAPHICAL SKETCH

Author: Meng Cui

Degree: Master of Science

Date: August 2008

Undergraduate and Graduate Education:

- Master of Science in Mechanical Engineering
  New Jersey Institute of Technology, Newark, NJ, 2008

- Bachelor of Science in Mechanical Engineering
  New Jersey Institute of Technology, Newark, NJ, 2006

Major: Mechanical Engineering

To my parents.

ACKNOWLEDGMENT

I would like to express my sincere gratitude to my thesis advisor Dr. Anthony Rosato, for guidance and support throughout this research. Special thanks are given Dr. David Horntrop and Dr. Ian S. Fischer for their active participation in my thesis committee. Author is also thankful to Shawn Chester, Olecksandr M. Dybenko, and Vishagan Ratnaswamy, who have diligently worked with me in the Granular Science Laboratory and helped review and discuss the various aspects of this thesis. I am glad to recognize the efforts of Demitrios Stamatis and Ervin Beloni, for their suggestions and generous support and help during the writing of this thesis. Lastly, I would like to thank my loved one, Ashley Chen, who gave me much support during this research.

TABLE OF CONTENTS

TABLE OF CONTENTS
(Continued)

Chapter **Page**

LIST OF TABLES

LIST OF FIGURES

LIST OF FIGURES
(Continued)

LIST OF FIGURES
(Continued)

LIST OF FIGURES
(Continued)

LIST OF SYMBOLS

d	Particle diameter
D	Cylinder diameter
ϕ	$\phi \equiv D/d$, Diameter ratio
ν	Solids fraction
σ_{rr}	Radial stress
σ_{yy}	Vertical stress
τ_w	Wall shear stress
K	Janssen constant
μ_w	Limiting wall-particle friction coefficient
μ_p	Limiting particle-particle friction coefficient
ρ	Particle mass density
$\underset{\sim}{F}_N$	Normal contact force vector
$\underset{\sim}{F}_T$	Tangential contact force vector
K_1	Normal loading stiffness
K_2	Normal unloading stiffness
α	Relative overlap between contacting bodies
$\underset{\sim}{x}_i$	Position vector of particle i
Δt	Time step
$\underset{\sim}{F}_{ij}$	Net force vector acting on particle i due to particle j
$\underset{\sim}{e}_r$	Unit vector from cylinder axis to contact point of two particles

$\underset{\approx}{P}$	Stress tensor
P_{yy}	Axial component of the stress tensor
P_{rr}	Radial component of the stress tensor
$<P_{rr}>$	Average radial component of the stress tensor
K_A	Janssen's constant for the active case
K_P	Janssen's constant for the passive case
F_y	Actual computed piston load in Newton's
F^*	$F^* \equiv \frac{6F_z}{\rho g \pi d^3}$, Piston force normalized by a single particle weight
$\hat{F}$	$\hat{F} \equiv \frac{F_z}{m_{total} g}$, Piston force as a fraction of the material weight
$< P_{rr}^* >$	$< P_{rr}^* >= \frac{P_{rr}}{P_{yy}}$, Average radial pressure normalized by normal pressure

CHAPTER 1

INTRODUCTION AND SIMULATION

1.1 Overview

Granular materials are large conglomerations of discrete particles. In general, granular materials behave differently from any of the other standard and familiar forms of matter, such as solid, liquid, and gas. Studies of granular materials are of great interest to industries because such understanding can be greatly beneficial in a variety of industrial processes, such as mining, agriculture, civil engineering and pharmaceutical manufacturing. The study of granular materials is also important for geological processes where landslides and erosion are a significant part of the morphology of the earth. However, understanding the behavior of granular flow is extremely difficult because of the properties and complexity of granular materials.

Despite the fact that the measurement of many physical quantities in granular flows is difficult in experimental studies, computer simulation allows us readily to obtain the quantities such as position, force, and pressure. Dr. Otis Walton and Robert Braun [11-15] of Lawrence Livermore National Laboratory developed a computer simulation code to study the uniform shearing flows. The code was later modified to include cylindrical boundary [13]. As part of this thesis, a major alteration in the computation of solid fraction profile, as well as the stress in radial direction, was developed.

An important aspect in understanding granular materials for a vertical cylinder is the use of Janssen's Theory [4, 10]. The theory not only predicts the dynamics of the asymmetric flows, but also is heavily used in industrial design. In most experimental

studies, small scale cylinders are used because they allowed for easy measurement of the materials. However, in this study, the results will not only be compared with the experimental data that have been published, but also with results from other simulations that were published in the literature. This thesis studies the pressure distribution in radial direction in a column of granular material, and the pressure profile along the cylinder wall. The results obtained in this study are in good agreement with the numerical data and experiments in the published literature.

1.2 Janssen's Theory

In 1895, H.A. Janssen [11] discovered that in a vertical cylinder, the pressure measured at the bottom does not depend upon the height of the filling; this is in contrast to Newtonian fluids at rest where the pressure is proportional to the fill height. This theory is very important in the framework of silo building, as the difference between ordinary hydrostatic and granular hydrostatic is mainly due to the presence of the force exerted against the walls of the cylinder. Janssen's model has four assumptions [23].

1. The vertical pressure is constant in the horizontal plane.
2. The horizontal pressure is proportional to the vertical pressure, such that $\sigma_{rr} = K\sigma_{yy}$.
3. Frictional forces are fully 'activated' at the wall.
4. The density of the material is constant throughout the depths.

Despite the fact that some of the assumptions in the Janssen's model are not valid in practical situations, most of industrial design is still based on his model because it

predicts the behavior of granular beds without using heavy calculations. It is well known for asymmetric flows that the stresses can be a large value which exceeds the value predicted by Janssen's model. Therefore, most industrial designs have been modified depending on specific needs.

To begin, let us look at the basic concept of stress acting on a cuboid.

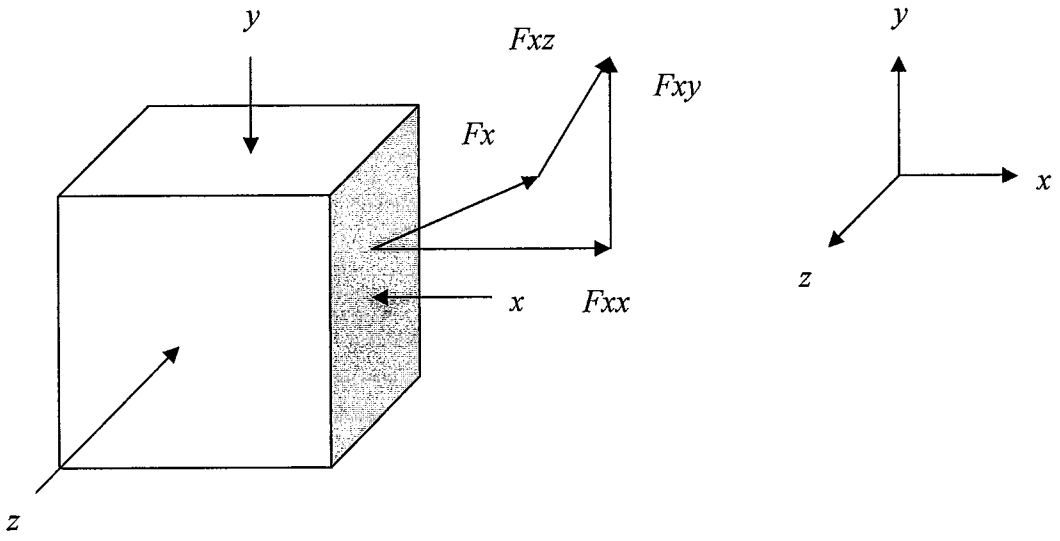

Figure 1.1 Force acting on an elementary cuboid parallel to the co-ordinate directions. *Fx* is force acting on *x* direction. *Fxx*, *Fxy* and *Fxz* are the forces acting on the x direction in three co-ordinate components.

Figure 1.1 shows the force acting on the cuboid parallel to each face of the cuboid. To be consistent, the name of the forces acting on each face of the cuboid is according to the directions of their normals; therefore there are two faces on *x, y,* and *z* directions. The force acting on the cuboid does not necessarily have to be normal to the each face. In Figure 1.1, the force acting in the *x* direction, *Fx*, can broke into three components in the three co-ordinate directions, *Fxx, Fxy,* and *Fxz*. To obtain the stress on the *x* direction, divide the area of the cuboid face, *Ax*, and usually we call it normal stress σ_{xx}, obtained from *Fxx* and the other two stresses which are called shear stresses τ_{xy}, τ_{xz}, obtained from

Fxy and *Fxz*. The stresses from the other two directions can be found in a similar manner. Since force is a three dimensional vector, therefore stress has nine components and cannot be a vector; these components are shown below in Equation (1.1).

$$\begin{bmatrix} \sigma_{xx} & \tau_{xy} & \tau_{xz} \\ \tau_{yz} & \sigma_{yy} & \tau_{yz} \\ \tau_{zx} & \tau_{zy} & \sigma_{zz} \end{bmatrix} \tag{1.1}$$

Consider an inclined surface with a block on it, as depicted in Figure 1.2. To prevent the block from slipping down the plane, P must be greater than $Mg\sin\alpha - \mu Mg\cos\alpha$. If P is required to pull the block up the plane, P must be less than $Mg\sin\alpha + \mu Mg\cos\alpha$.

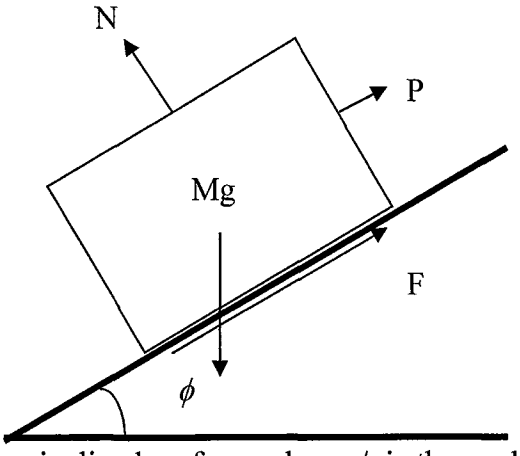

Figure 1.2 Block on an inclined surface; where ϕ is the angle of the inclined surface N is the normal to the block, Mg is the weight of the block, F is the frictional force and P is the applied force.

From above we can see that if the stress on the inclined surface is pushed downwards by the block, it is called 'Active Stress'. Similarly when the force pulls the block upwards on the incline, it is called 'Passive Stress'. More detailed information on this topic can be found on [23].

When considering an active state as above, one can use the Mohr-Coulomb diagram in Figure 1.3 to provide the basis of failure analysis. Here, $P^* = \frac{1}{2}(\sigma_{xx} + \sigma_{yy})$, and $R = p^* \sin\phi$.

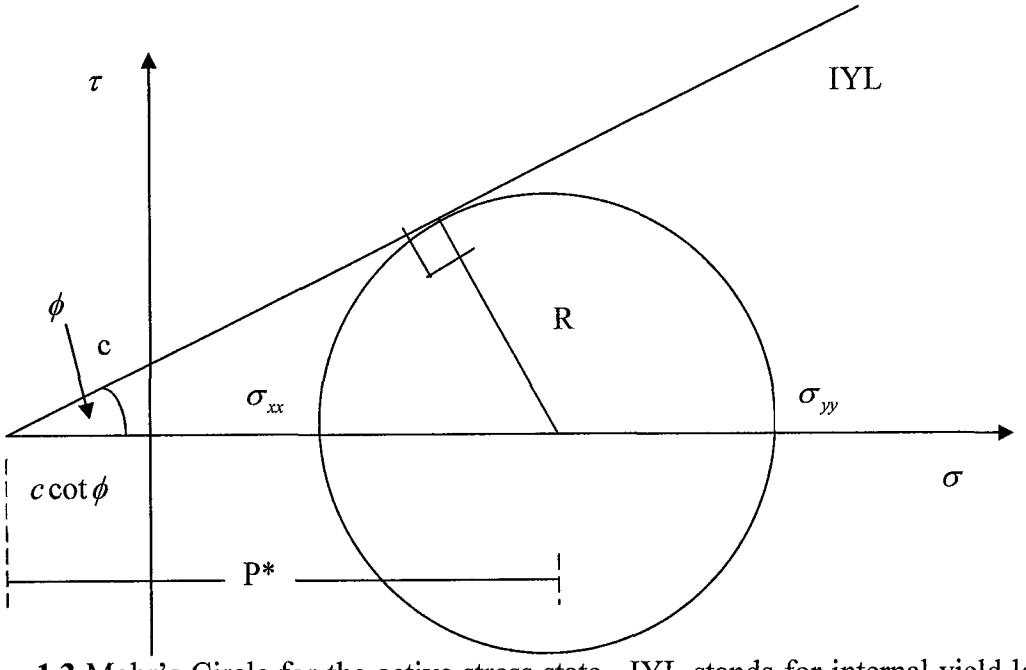

Figure 1.3 Mohr's Circle for the active stress state. IYL stands for internal yield locus. If is cohesionless material, the c becomes zero.

The Mohr's Circle shows that the stress on the axial direction σ_{yy} is defined as:

$$\sigma_{yy} = P^* + R - c\cot\phi \tag{1.2}$$

$$\sigma_{xx} = P^* - R - c\cot\phi \tag{1.3}$$

We know that σ_{xx} is the active stress on the inclined surface which is the horizontal stress, and σ_{yy} is the vertical stress. In this thesis, the horizontal surface is the radial direction pointing to the wall and the vertical direction is the direction along the cylindrical wall; see Figure 1.4.

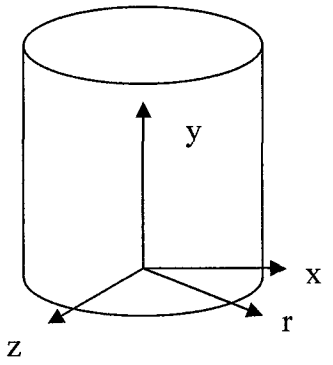

Figure 1.4 Co-ordinate system in the cylinder. y is the vertical and x is the horizontal direction of the cylinder.

Therefore, $\sigma_{rr} = \sigma_{xx}$ and by eliminating P* in equation (1.2) and (1.3) gives us:

$$\sigma_{rr} = \frac{1-\sin\phi}{1+\sin\phi}\sigma_{yy} - 2c\frac{\cos\phi}{1+\sin\phi} \tag{1.4}$$

In the case of cohesionless material, c goes to zero, and the equation then becomes:

$$\sigma_{rr} = K\sigma_{yy} \tag{1.5}$$

where K is defined as $K = \frac{1-\sin\phi}{1+\sin\phi}$. The K is known as Rankine's coefficient of active earth pressure [23]. A similar analysis can be found in a passive case where $\sigma_{rr} > \sigma_{yy}$, which gives us:

$$\sigma_{rr} = \frac{1+\sin\phi}{1-\sin\phi}\sigma_{yy} + 2c\frac{\cos\phi}{1-\sin\phi} \tag{1.6}$$

and the coefficient of passive earth pressure K is defined as $K = \frac{1+\sin\phi}{1-\sin\phi}$.

1.3 Review of Published Literature

H.A. Janssen [11] was the first person who gave a theoretical model for vertical pressure profile in a granular column. More then 330 published papers have cited Janssen since

1980 [6]. Nedderman [23], who studied Janssen's prediction, points out two debatable assumptions. One is that the axial and radial stresses are proportional to each other by a value K, equation (1.5). The second assumption is that the stress across any horizontal cross sections is uniform [23].

In 1992, Mueller published an article based on experiments using X-ray radiography to determine radial void fraction distributions in randomly packed fixed beds of mono-sized spheres in cylindrical containers [20]. In his article, he used geometrical analysis and presented analytical equations which were used to obtain the radial void fraction distributions. Mueller has proposed an approximate radial distribution with a Bessel function of first kind,

$$\varepsilon(r) = 0.365 + \frac{0.22}{\frac{D}{d}} + \left(1 - 0.365 + \frac{0.22}{\frac{D}{d}}\right) J_0 \times \left(\left(7.45 - \frac{3.15}{\frac{D}{d}}\right)\frac{r}{d}\right) \exp\left(-\left(0.315 - \frac{0.725}{\frac{D}{d}}\right)\frac{r}{d}\right) \qquad (1.3.1)$$

His analysis presented an analytical equation and nondestructive method to determine the radial void fraction distribution for uniformly sized spheres in cylindrical containers. However, using X-ray radiography to determine the center of particle coordinates will not be practical for larger models.

In 1996, Mueller extended his 1992 results through the use of numerical simulation. Numerical simulation is easier than experiments when creating and reproducing random packing of spheres for any diameter aspect ratio and accurately determining their coordinates [22]. The precision in determining the sphere position is only limited by the computer's accuracy. Mueller used a range of six diameter aspect

ratios to compare with the models; he concluded the model had a low percentage standard error compared with numerical models and experimental data.

A group of Brazilian chemists used the Monte Carlo method to simulate the packing and segregation of spheres in cylinders [20]. The simulations were performed in three different diameters aspect ratio (D/d). The results showed the local void fraction as a function of the distance from the cylinder wall are averages of five replicated computational experiments done by Mueller. They also showed that the Monte Carlo method can also be used to calculate positions of the particles in the cylinder accurately.

In 2006, J. Theuerkauf, P. Witt, and D. Schwesig used the discrete element method to determine the porosity distribution of spherical particles in narrow pipes as a function of the pipe-to particle diameter ratio [10]. In conclusion to their results, the DEM simulation could correctly generate distribution of the particles in the tube regardless of the diameter ratio.

In 2003, Landry and Grest [16] published a paper that illustrated a variety of methods to generate the packing and studied the effects of packing preparation on the final static packing. Landry showed that the Janssen's analysis does not describe their results, and therefore modification was needed. However, they have shown that the majority of the particles who have wall contact forces in the bulk were at or near the Coulomb failure limit; the particle contact with the particles were far from the limit.

In 2004, Walton [12] completed some experiments using 3 mm glass beads in a 4 cm acrylic tube with a diameter ratio of D/d = 13.3. The results verified the exponential functional forms of Janssen's model. Walton's findings are interesting because the radial stress (times the friction coefficient) against the applied axial stress has a linear variation

relationship. However, the line does not intersect the origin in accordance with Janssen's assumption given by Equation (1.5).

The study of floor pressure induced by a granular column in a cylindrical container was done by Chester [6]. He studied the load on a piston supporting a monodisperse granular material which consisted of friction and inelastic spheres within a cylindrical vessel. He used the discrete element simulation to evaluate the friction of the wall by moving the piston as well as the cylinder wall slowly downwards. By using different values of wall friction, he discovered that a translation of either the floor piston or the cylinder wall will affect the load and fill height behavior.

In Janssen's assumption, the lateral stress is a fixed fraction of the axial stress. This may not be true because Chester [6] expected that elastic solid would exhibit such behavior and a granular assembly would fail at the Coulomb failure limit. Additionally, the stress distribution across the horizontal layer could not be uniform in a granular assembly as Janssen stated otherwise. This study opens the door to compute the radial stress and axial stress as a function of both radial and axial location, and to verify whether or not Janssen's assumption of stress across any horizontal layers is uniform.

1.4 Objective

In this thesis, the investigation of the axial and average radial pressure in a cylindrical vessel with inelastic spheres is done via discrete element simulations (DEM). A relatively small diameter ratio D/d = 13.33 is selected to enable the comparison of the results with experiments and published data, where D is the diameter of cylindrical vessel and d is the diameter of the spheres. The radial solid fraction v is also studied in order to

compute the average radial pressure. Varying diameter ratios D/d are selected in these cases to verify the reliability of the computation in comparison to the published literature. The normal pressure on the piston is also investigated to support the calculation of average radial pressure. The goal of the simulations is to validate the assumptions in Janssen's theory, and discuss the results within the framework of these assumptions.

1.5 Thesis Outline

This thesis is organized with Chapter One the introduction, Chapter Two the description of the dynamics simulation, Chapter Three the introduction of the force model, Chapter Four the calculations of the volume fraction and validation to support average radial pressure, Chapter Five the overview of the average radial pressure and simulation results and lastly Chapter Six the conclusion and further work.

CHAPTER 2

PARTICLE DYNAMICS SIMULATION

2.1 Discrete Element Method (DEM) Simulation

The discrete element method (DEM) is a family of numerical methods for computing the motion of a large number of particles. The method was introduced by Cundall in 1971 to study the behavior of a system containing granular particles [21]. A computer simulation is developed in here to find the particle's trajectories, velocities, and other quantities which help in understanding the behavior of granular materials. For the most part, dynamic simulation has been a powerful tool to examine the relationships between the motion of individual particles and material properties.

2.2 Overview of the Particle Dynamics Simulation

The computer simulation used in this thesis has considered smooth, inelastic, and uniform spheres in a cylindrical boundary. Figure 2.1 shows the initial coordinates of particles in a cylinder are randomly generated, and the algorithm to prevent forbidden overlaps is detailed in [12].

The DEM code has been many modifications since its first development by Walton and Braun [13]. The rectangular geometry with an oscillating floor was modified to a cylindrical geometry with a moving piston and moving cylinder wall in this study. The main program, *3shear.f*, will read input file first. The subroutine *dumpread.f* will read the file from previous simulation to continue the simulation if the previous

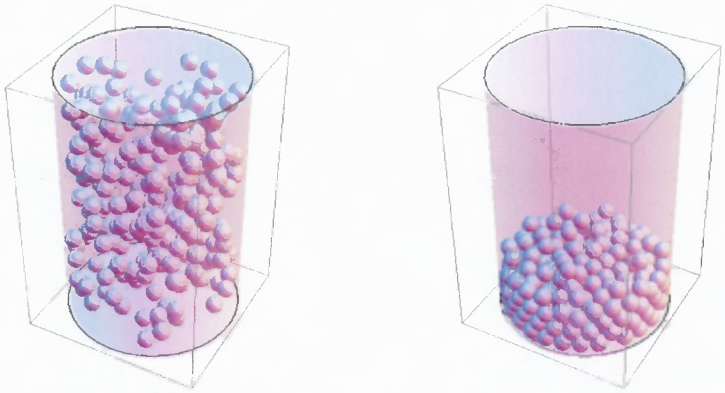

Figure 2.1 Demonstration of a Dynamics Simulation. The system first randomly dumps the particles into the cylinder, and then the particles fall down by activating gravitational force.

computation is interrupted or stopped by the user. The subroutine *init.f* will initialize the simulation; in addition, *bound.f* will be called for initialization of boundaries conditions. After all the particles' initial positions are randomly generated, subroutine *findrad.f* then assigns the particles dimension. If two of the simulation particles are overlapping each other or with a boundary, then the simulation will stop. Subroutine *initcum1.f* and *initcum2.f* will initialize the short and long term cumulative averages.

Once all of the particles and boundaries are initialized, the simulation will begin. The subroutine, *update.f,* will create the linked list of near neighbors. This linked list will create a search radius and if one or more particles falls into this search radius, these particles will become neighbors. Furthermore, subroutine, *deletem.f,* will be called to remove particles from the linked list if particles traveled outside the search radius. The next section will talk more on the linked list.

After the initialization, the subroutine, *initstep.f,* will be called to initialize parameters for computing the particle's forces and the integration routines. The subroutine *forces.f* will be called to compute the particle force due to contacts using the

force model. For more information on force model, please refer to Chapter 3, Section 1. After the calculation of contact force, the subroutine *integ1.f* will compute the velocities at the current time step for the particle. The next subroutine *diagnos2.f* computes the potential component of the stress tensor at the current time step. The last thing the simulation will perform is writing data through subroutine *datasav2.f.* After all the process is done, the simulation will start over at the next time step.

2.3 Description of code

Figure 2.2 contains a flow chart of the code used in this thesis. In this section, the subroutines are described in detail with their functions.

bound.f

This subroutine is used to assign coordinates, velocities and other parameters for boundary particles. The user has to input the number of boundary particles.

datain.f

This subroutine reads the input file from "i3ds."

datasav2.f

This subroutine writes the output file with the user defined perimeters.

deletm.f

This subroutine loops the entire particle near neighbors in the linked list and removes near neighbors if particles are beyond the distance of radius.

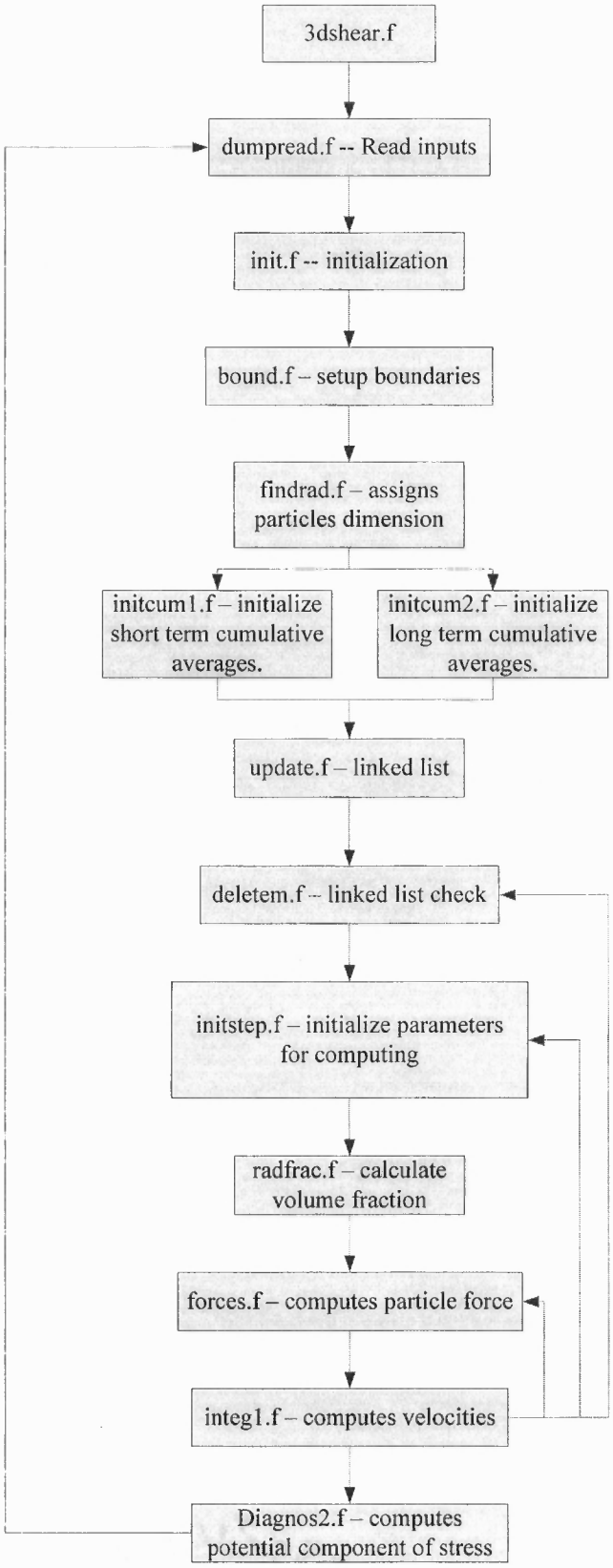

Figure 2.2 Main program flow chart.

diagnos2.f

This subroutine calculates simulation diagnostics locally and globally. The kinetic contribution to the stress tensor is also calculated in this routine.

dumpread.f

This subroutine is used to restart a simulation. All the information from a previous simulation is stored in "d3ds."

findrad.f

This subroutine assigns the particle radii at time zero and increases radii each time step until it reaches the predetermined value.

forces.f

This subroutine calculates the inter-particle forces between particles. The force model used in this routine is the spring model.

init.f

This subroutine initializes the simulation. Initial coordinates and fluctuation velocities of particles in the system are generated.

initcum1.f

This subroutine initializes the short term variables.

initcum2.f

This subroutine initializes the long term variables.

initstep.f

This subroutine initializes the integration step.

integ1.f

This subroutine performs an integration of the velocity equations in the current time step.

integ2.f

This subroutine calculates the coordinates of particles at each time step as well as the velocities.

update.f

This subroutine updates the list of particle neighbors and prevents overlaps.

vodfrac.f

This subroutine calculates fraction volume of a particle. In order to calculate the radial stress component, this fraction volume is needed in the subroutine diagnos2.

2.4 Linked List Logic

The basic idea behind the linked list is a simple contact detection process. This process involves the particle's position and geometry in order to check if the particles are against each other. This process also reduces the computational work which is required to determine the motions of particles.

The detection process starts with one particle *i* inside of a system of particles. This particle *i* will be restricted to a search volume around the particle, and the radius of this volume is called the search radius. Therefore, instead of finding all of the particles that interact with particle *i,* the system only needs to find a small number of particles

within the range of the search volume. This process reduces much of computational time when the system contains a very large number of particles. The linked list continues to track all the particle's near neighbor and update the particle's linked list with required time until the simulation is done. More detailed information about the linked list can be found in [13].

2.5 Force Model

The force model that used to simulate the particle collisions is a soft sphere approach where collisions occur over a finite length of time. This force model was developed by Walton and Braun [2, 3] and it is a partially latching spring model. The model allows the contacting particles to slightly overlap and a linear stiffness in the force model computes a contact force in proportion to the amount of overlap. Also, any particle in the system may be in contact with other particles nearby at the same time. The vector sum of the all normal and tangential forces on the particle is the net force.

The normal force model incorporates two different normal stiffnesses; loading (K_1) and unloading (K_2). The magnitude of the normal force is given by Equation (2.1) below.

$$F_N = \begin{Bmatrix} K_1\alpha \\ K_2(\alpha - \alpha_o) \end{Bmatrix} \tag{2.1}$$

Where α is a function of the relative overlap between colliding particles, and α_o is the remaining overlap at which point the unloading force goes to zero due to plastic

deformation of the contact. Therefore, the model gives a constant coefficient of restitution e shown in Equation (2.2).

$$e = \sqrt{\frac{K_1}{K_2}} \tag{2.2}$$

Additionally, K_1 can be expressed through a Hertzian contact analysis given by Equation (2.3).

$$K_1 = \left\{ \frac{4E\sqrt{dv_{\max}}}{15m(1-v^2)} \right\}^{4/5} \tag{2.3}$$

where E is the elastic modulus, v is the Poisson ratio, d is the diameter of the particle, m is the mass of the particle and v_{max} is the maximum estimated impact velocity.

The tangential force model developed by Walton and Braun is based on Mindlin's theory [15] via contact stiffness K_T that decreases with displacement until full sliding occurs at the friction limit.

$$K_T = \begin{Bmatrix} K_o\left(1-\dfrac{F_T - F_T^*}{\mu N - F_T^*}\right)^{1/3} \\ K_o\left(1-\dfrac{F_T^* - F_T}{\mu N + F_T^*}\right)^{1/3} \end{Bmatrix} \tag{2.4}$$

Equation (2.4) shows the effective tangential stiffness K_T, where F_T is the total tangential force, μ is the coefficient of friction, N is the total normal force, and F_T^* is the loading reversal value.

The net force due to collision with two particles i and j is the vector sum of the normal and tangential contact forces described above. The net contact force acting on the contacting particle is given by Equation (2.5).

$$\underset{\sim}{F}_{ij} = \underset{\sim}{F}_N + \underset{\sim}{F}_T \tag{2.5}$$

Further details about the force model are presented in [2, 3].

CHAPTER 3

AVERAGE RADIAL PRESSURE CALCULATION

3.1 Overview of Average Radial Pressure Calculation

This section describes the calculation of average radial pressure as used in later chapters. Note that instead of radial pressure this study calculates the average radial pressure. There are three types of calculations of average radial pressure carried out in this thesis;

a. Average radial pressure in a whole cylinder.

b. Average radial pressure in horizontal cross sections of the cylinder.

c. Average radial pressure in vertical cross sections of the cylinder.

These types of calculation can be illustrated in Figure 3.1.

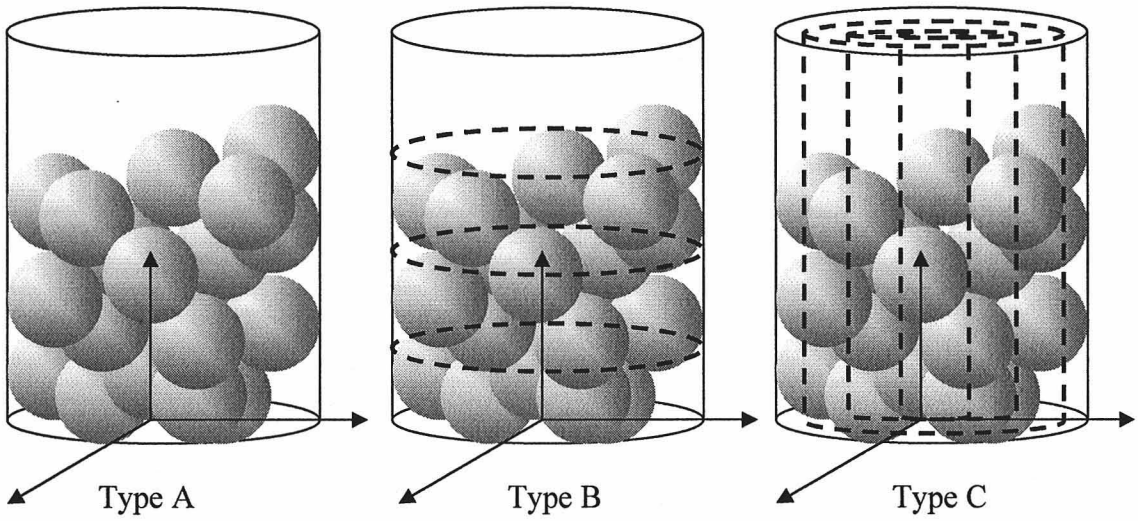

Figure 3.1 Illustration of three types of average radial pressure calculation. Type A is the average radial pressure in a whole cylinder. Type B is the average radial pressure in horizontal cross sections of the cylinder. Type C is the average radial pressure in vertical cross sections of the cylinder.

Type A pressure calculation contains the study of average radial pressure versus fill height (H/D), average radial pressure versus time, and average radial pressure versus

normal pressure. Type B pressure calculation contains the study of average radial pressure in horizontal cross sections versus height of the cylinder and average radial pressure of 4 diameters height from the bottom of the cylinder versus time. Type C pressure calculation contains the study of average radial pressure in vertical cross section versus the width of cylinder and the average radial pressure in vertical cross section versus time. These studies help to understand the behavior of the granular materials in a cylinder.

The granular materials have two components; these are known as the kinetic component and the potential component. Because the motion in this thesis is quasi-static, the kinetic component of the pressure tensor is negligible. The general form of pressure tensor in Cartesian coordinates is

$$P = \begin{bmatrix} P_{xx} & P_{xy} & P_{xz} \\ P_{yx} & P_{yy} & P_{yz} \\ P_{zx} & P_{zy} & P_{zz} \end{bmatrix} \tag{3.1}$$

In order to validate the main assumptions of the Janssen's theory, $P_{rr} = KP_{yy}$ where P_{rr} is radial pressure and P_{yy} is the normal pressure, the calculation of the radial stress F_r is needed. The radial pressure in Cartesian coordinates can be computed as,

$$\underset{\sim}{P}_p = \frac{1}{V} \sum_{j \neq i} \underset{\sim}{F}_{ij} \underset{\sim}{R}_{ij} \tag{3.2}$$

However, the radial pressure that was calculated in this thesis is in cylindrical coordinates. Also the total force of the particle used to calculate the pressure is given in Cartesian coordinates; therefore, coordinate conversion is needed. Consider a cylinder

with Cartesian coordinates in Figure 3.2, where $\underset{\sim}{e}_r$ is the radial direction needed to calculate the radial pressure.

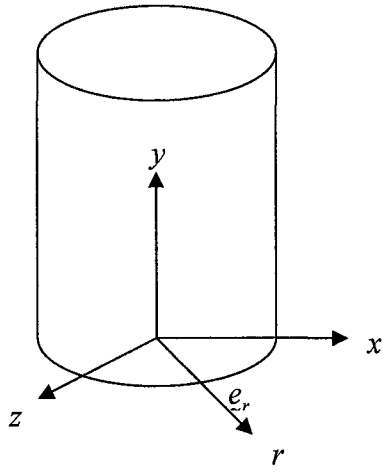

Figure 3.2 Cartesian coordinates x, z, and y represented in a cylinder, and the cylindrical coordinates is represented by direction r.

The computation of the P_{rr} involves the contact force between the two particles i and j in the radial direction F_r and can be calculated as $\underset{\sim}{F}_r = (\underset{\sim}{F} \bullet \underset{\sim}{e}_r)\underset{\sim}{e}_r$ and is given by

$$\underset{\sim}{F}_r = (F_x \bullet \underset{\sim}{e}_r + F_z \bullet \underset{\sim}{e}_r)\underset{\sim}{e}_r \tag{3.3}$$

where F_x and F_z is the force acting on the particles in x and z directions in Cartesian coordinates. These two forces can be calculated from the total contact force between the two particles. The unit vector of the radial direction is between the cylindrical axis and the contact point of particle i and j. The unit victor can be calculated by

$$\underset{\sim}{e}_r = (\underset{\sim}{e}_c \bullet \underset{\sim}{e}_x)\underset{\sim}{e}_x + (\underset{\sim}{e}_c \bullet \underset{\sim}{e}_z)\underset{\sim}{e}_z = \frac{\left(\frac{x_i + x_j}{2}\right)\underset{\sim}{e}_x + \left(\frac{z_i + z_j}{2}\right)\underset{\sim}{e}_z}{\sqrt{\left(\frac{x_i + x_j}{2}\right)^2 + \left(\frac{y_i + y_j}{2}\right)^2 \left(\frac{z_i + z_j}{2}\right)^2}} \tag{3.4}$$

and now the radial force between the two contact particle i and j can be written as,

$$\underset{\sim}{F}_r = \left(\frac{F_x\left(\frac{x_i + x_j}{2}\right) + F_z\left(\frac{z_i + z_j}{2}\right)}{\sqrt{\left(\frac{x_i + x_j}{2}\right)^2 + \left(\frac{y_i + y_j}{2}\right)^2 \left(\frac{z_i + z_j}{2}\right)^2}} \right) \underset{\sim}{e}_r \tag{3.5}$$

Figure 3.3 below shows the F_r in the cylindrical coordinates.

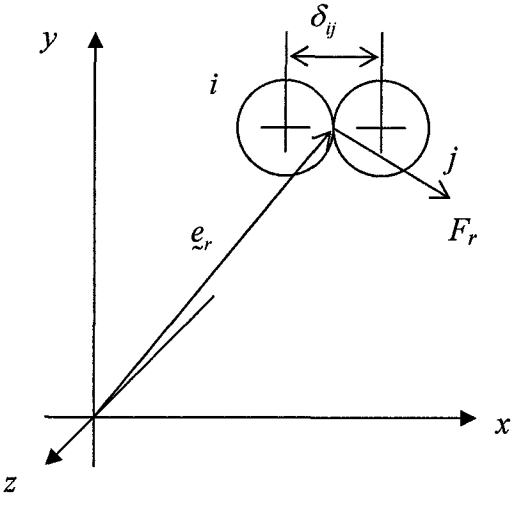

Figure 3.3 Cylindrical coordinate for particle i and j in contact. The radial contact force is represented as F_r and the direction of the radial contact force is represented as $\underset{\sim}{e}_r$.

The radial distance between the centers of the colliding particles i and j is given by,

$$\delta_{ij} = \sqrt{x_j^2 + z_j^2} - \sqrt{x_i^2 + z_i^2} \tag{3.6}$$

Recall that in a cylindrical coordinate, $\underset{\sim}{R} = R_\theta \underset{\sim}{e}_\theta + R_r \underset{\sim}{e}_r + R_y \underset{\sim}{e}_y$; therefore the r direction component becomes $R_r = \delta_{ij}$. The computation of the P_{rr} is completed by Equation (3.7), where V is the control volume over which averaging takes place.

$$p^*_{rr} = \frac{1}{V} F_r \delta_{ij} \tag{3.7}$$

Here the calculation of the radial pressure is only true for two particles in contact. However, Equation (3.7) only applies when the two particles are totally inside the control

volume. In the case of type B pressure calculations, shown in Figure 3.1, the cylinder has horizontal cross section cut and the resultant shape becomes a shorter cylinder. The other control volume is in type C pressure calculation where the cylinder has vertical cross section cut and the resultant shape becomes a pipe with thick wall. Equation (3.7) shows that F_r is the radial direction contact force between the two particles. However, if one particle partially outside the control volume is in contact with the other particle totally inside the control volume (see Figure 3.4), the volume fraction will be added to Equation (3.7) becomes $p^*_{rr} = \frac{1}{V} v F_r \delta_{ij}$, where v is the volume fraction.

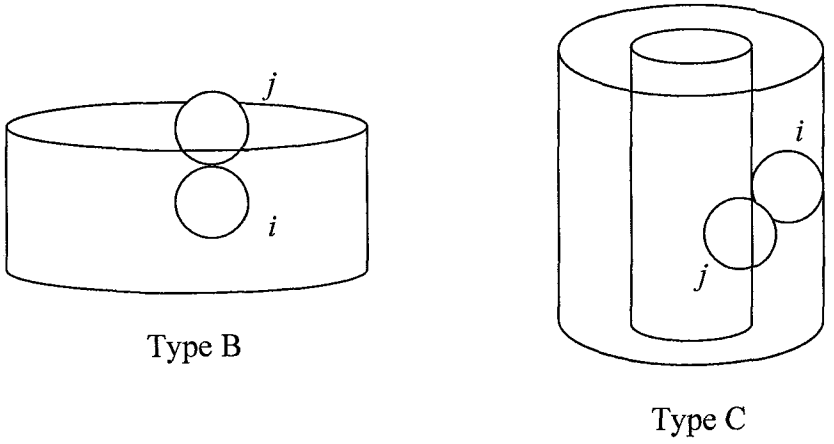

Figure 3.4 Particle i and j are in contact, and particle j in both Type B and Type C are partially outside the control volume; therefore, volume fraction for particle j is needed.

After the calculation of the radial pressure of two particles in contact, this calculation will repeat itself until all the pairs of particles in contact in the system are counted. The radial pressure of all the particles then added to form the average radial pressure of the control volume,

$$\langle P_{rr} \rangle = \frac{1}{V} \sum v F_r \delta_{ij} \tag{3.8}$$

where $\langle P_{rr} \rangle$ is the average radial pressure of the control volume.

3.2 Volume Fraction

The fraction, v, in equation (3.8) is the control volume fraction of the particles in the specified region. In the calculation of radial pressure, such fraction is difficult to determine. As Figure 3.5 demonstrates, the shaded area that is used to calculate the radial pressure can be a disc cylinder, and the control volume is the volume of the particles inside this shaded area. Because the partial volumes of some particles are not completely found inside the shaded region, the only volume required to determine the radial pressure is the partial volume of the particles inside this region. This is useful when one wants to study a particular region inside the cylinder.

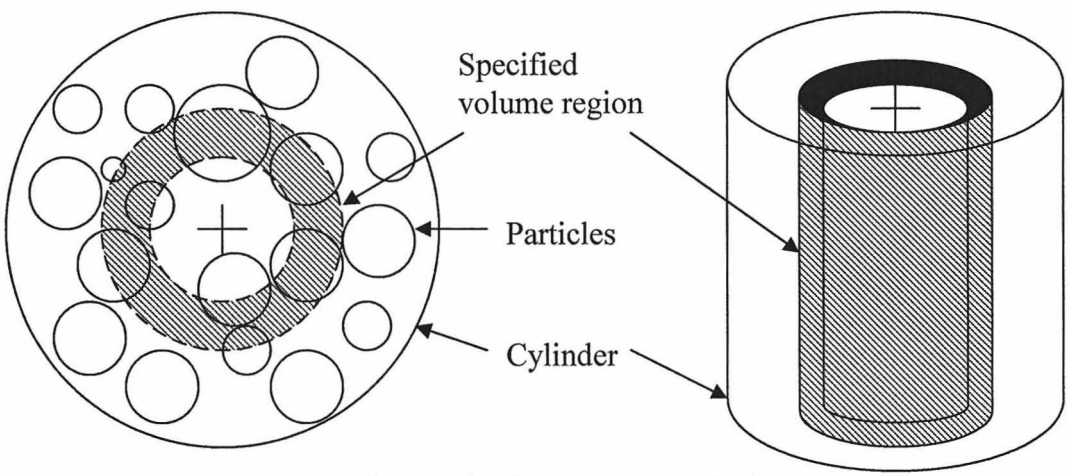

Figure 3.5 Demonstration of control volume in a specified region in a cylinder. The shaded area is the specified volume region where the calculations are taking place.

In cylindrical packed beds systems, the calculations of the control volume were computed by using arc-length intersection method which simply is the calculation of arc-length of two intersecting circles. First, the cylinder is cut into cross sections. On one of the cross sections, various circles are defined from the inner circumference to the outer circumference of the shaded region. Second, the arc-length intersection calculation is then performed between the various circles defined from the previous step and the

particle radius inside the circumference of the shaded region. Next, the calculated arc-length between these circles and particles are added together to form the area. The control volume is found by multiplying the area by a finite height. The height, Δy, is a user defined quantity, and the accuracy of the results depends on the size of this value. This calculation then repeats itself until the volume of the solid in that cross section no longer belongs to the specified region. For detailed information of how the control volume calculated, please refer to the next section of this thesis.

An analytical and general expression of the "Calculation of the Volume Intersection in an infinite cylinder and a sphere" was presented by Lamarche and Leroy (1990) [14]. Lamarche and Leroy utilized "Volume Cross-section" method to measure the control volume in the cylinder. However, the use of this expression requires an approximation due to the introduction of the finite cylinder. The volume of the intersection is overestimated. On the other hand, Abreu (1999) presented a similar method but with a finite height structure. Because the complexities of these calculations, it requires more computing power [20]. Thus in this thesis, the arc-length intersection method is used.

3.3 Computation of the Arc-Length Intersection

This section presents an algorithm for calculating the circumference using the cylinder radius R and the sphere diameter d. The structure of the calculation is to specify the different zones first. The y-zone which consists of horizontal layers, and the r-zone, which is composed of the vertical cylindrical layers. The calculation begins with loops through the particles first, and then loops through the y-zone layers. The program will

loop the intervals Δy, which are user specified, in the y-zone layer to find the particle. After the particle is found, the computation of the arc-length intersection begins. Figure 3.6 shows the y-zone layer in a top-down view of the system. In order to measure the arc-length intersection, one of the conditions for it to existence is

$$|y - y_i| \leq \frac{r}{2} \tag{3.9}$$

where y is the cylinder height and y_i is the height of i^{th} particle. The r is the radius of the cylindrical layer, r-zone.

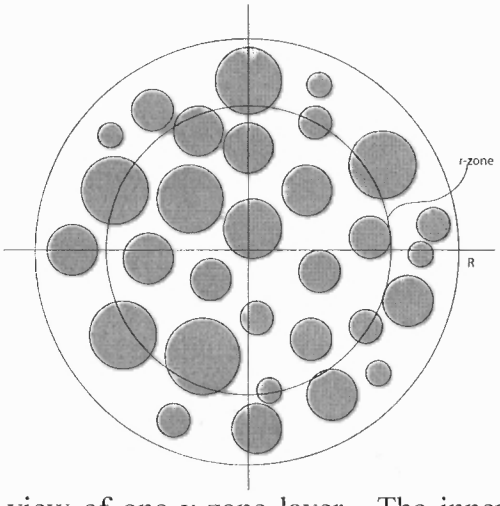

Figure 3.6 Top-down view of one y-zone layer. The inner circumference is the r-zone that one use to calculate the arc-length of the intersect particles.

The height of the intersection of the circumference parallel to the x, z plane is represented by

$$ylocation = ybot + \left(\left(j - 1\right) * \Delta y\right) \tag{3.10}$$

where *ylocation* is the height of the intersection circumference and *ybot* is the height of the bottom layer of the y-zone. The *ylocation* is needed to determine the radius of the particle that has been cut by the y-zone layer. The radius of the circle that corresponds to the horizontal section of particle i at height $y(i)$ is given,

$$rady = \sqrt{\left(\frac{r}{2}\right)^2 - \left(ylocation - y(i)\right)^2} \tag{3.11}$$

After calculating these quantities, one more step is needed to start measuring the partial volume; that is the verification of the existence of the intersection on the particle. There are total of four verification cases, and the intersection of the circle with particles does not always exist as shown below. The first case is when

$$r + rady \leq \sqrt{x_i^2 + z_i^2} \tag{3.12}$$

Figure 3.7 shows the circumference does not touch the particle hence, no intersection.

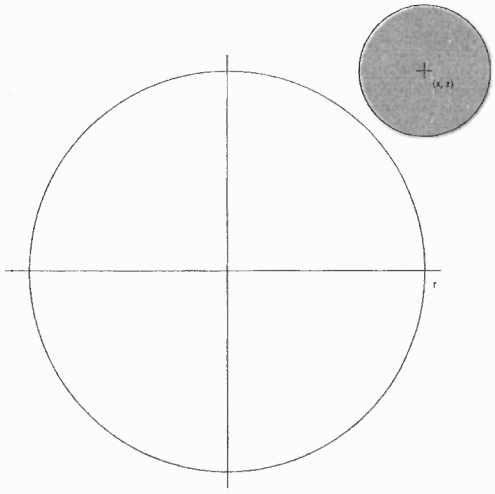

Figure 3.7 Verification Case 1 where $r + rady \leq \sqrt{x_i^2 + z_i^2}$, r is the circumference that one used to calculate the intersection and *rady* is the radius of the particle at height y_i.

The second case is when

$$r > rady \text{ and } r - rady \geq \sqrt{x_i^2 + z_i^2} \tag{3.13}$$

In this case, the particle is inside the circumference and the particle does not touch the outer circle; see figure 3.8, therefore, intersection does not exist.

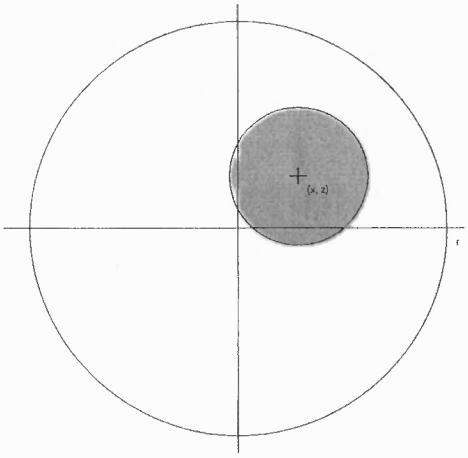

Figure 3.8 Verification Case 2 where $r > rady$ and $r - rady \geq \sqrt{x_i^2 + z_i^2}$. In this case the particle does not touch the intersection circle and therefore no calculation is needed.

The third case is when

$$r < rady \text{ and } rady - r \geq \sqrt{x_i^2 + y_i^2} \tag{3.14}$$

In this case, the circumference intercepts the whole particle; see figure 3.9. This only happens when a particle is near the center region of the cylinder, and user specified radius intervals, *deltar*, is less than the radius of the particle.

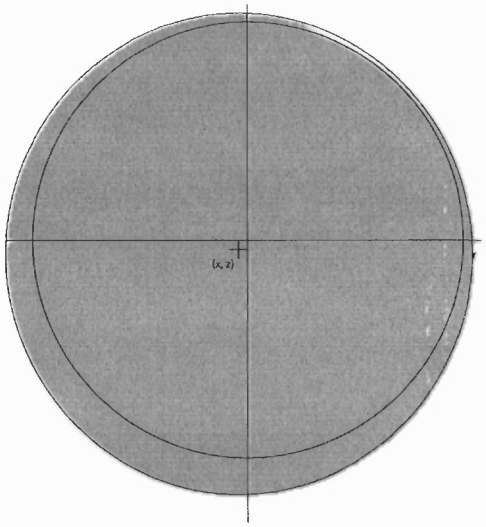

Figure 3.9 Verification Case 3 where $r < rady$ and $rady - r \geq \sqrt{x_i^2 + y_i^2}$. In this case the whole particle is being intersected by the circumference therefore the arc-length is simply $2\pi r$.

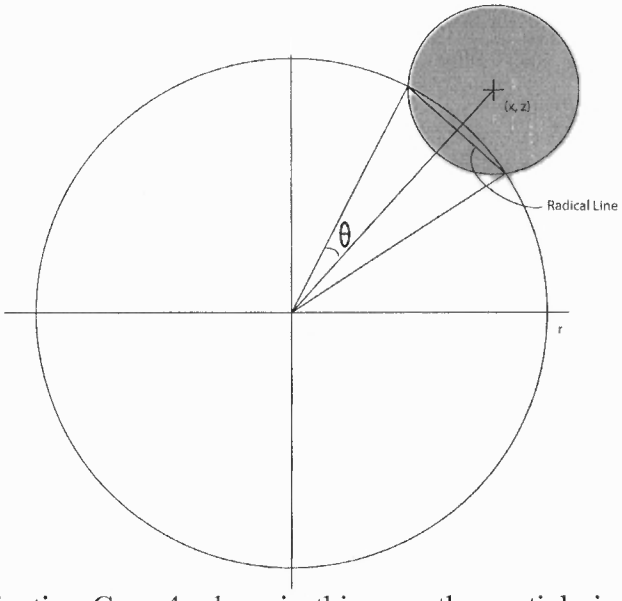

Figure 3.10 Verification Case 4 where in this case the particle is being intersected by the circumference and therefore the arc-length calculation is needed.

The last case is when only a fraction of the particle is intercepted by the circumference. In this situation, the calculation of circle-circle intersection is needed. The calculation of circle-circle intersection was done by Sloane [24]. The intersection of two circles determined by a line known as the radical line. The radical line can be calculated by using

$$a = \frac{1}{d}\sqrt{4d^2R^2 - (d^2 - r^2 + R^2)^2}\ . \tag{3.15}$$

where d is the diameter of the particle, r is the radius of the particle, and R is the circumference that intersects this particle. The line between the cylindrical shell center and the radical point on the particle is then found by using

$$x = \frac{d^2 - r^2 + R^2}{2d}. \tag{3.16}$$

Finally, the arc-length p is found using.

$$\theta = \arctan\left(0.5a/x\right) \text{ and } p = R \cdot \theta, \tag{3.17}$$

The next step after acquiring the arc-length is to calculate the area of the particle in the horizontal layer. The program continues to loop the intervals inside the r-zone and added all of the arc-length to form the area. Next this area is multiplied by the horizontal intervals Δy to form volume in that layer. The final step is to add all of the volume segments in the region to form the partial volume.

3.4 Comparison of Results

A force model calculation is presented below in Figure 3.11 that shows the force on the piston floor versus time. At time t equals to zero, there is no force on the floor; this is expected as the simulation just placed particles randomly in the cylinder and nothing is moving. Therefore, the force on the floor should be zero. Then, at time t equals to 1.9 seconds, there is floor force which indicates that the particles are starting to fall. Then around 3.5 seconds, the entire system settles rest on the piston floor and the force becomes the weight of the particles that is inside the cylinder.

In order to confirm that the calculation of the partial volume is correct, the total of the particle volumes has to match with the actual volume of the particle. Table 3.1 below shows the simulated parameters and the results, as well as the percentage errors compared with actual data. The particles that are used in this simulation have 0.0063mm in diameter and with D/d of 1.0, 2.3, 5.0 and 10.5 respectively to the number of particles. The H/D for the cylinder is 5 for all cases. The lowest percentage of errors falls into 1 yzone and 1 rzone, which is expected because the simulation does not calculate any intersections. The biggest percentage of errors is in 5 yzones and 5 rzones, these errors are believed to result from the integration method used in section 3.3.

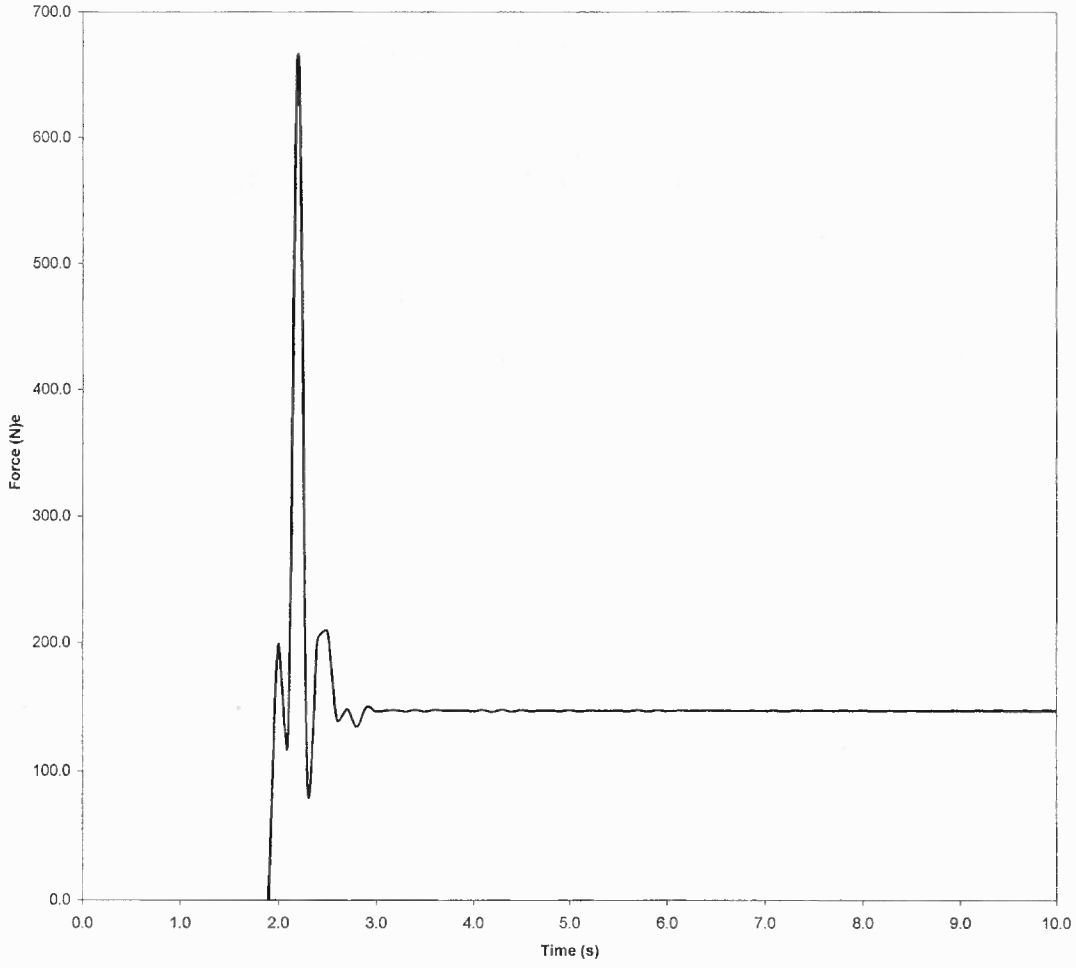

Figure 3.11 The black line represents the force on the piston floor over total time of 10 seconds. At time equals to zero, the system randomly placed particles in side the cylinder, then after 1.9 seconds, the gravitational force takes over and the particles fall to the floor of the cylinder.

Solid fraction and void fraction were calculated to provide further evidence that the arc-length intersection calculation is legitimate. Both calculations in the system contained identical spheres with diameter of 0.001 m, and the differences between these two systems were the number of particles with diameter aspect ratio (D/d) and the ratio of the fill height to the diameter of the cylinder (H/D).

Table 3.1 Simulated Parameters and the Results Compared with Actual Data.

# of Particles	1 yzones & 1 rzones	5 yzones & 5 rzones	20 yzones & 20 rzones
1	0.001086	0.001083	0.001086
errors compare with actual volume	0.00%	0.28%	0.00%
5	0.005429	0.005429	0.005417
errors compare with actual volume	0.00%	0.00%	0.22%
15	0.016286	0.016	0.01626
errors compare with actual volume	0.00%	1.80%	0.16%
50	0.054288	0.05353	0.05421
errors compare with actual volume	0.00%	1.39%	0.14%

Figure 3.12 below shows systems of diameter ratio D/d of 5.6, 13.4, 14.1 and 20.3, and fill height H/D of 5 in the cylinder. The solid fractions of these systems are around 0.6. The value of around 0.64 is found as an upper limit for the sphere volume fraction in a random close packing configuration [1]. However, our simulation gives 0.6 as expected because the configuration here is a loose packing, meaning the system randomly positioned the particles and let them rest by themselves. Also from the figures, there is a "spike" peak at the beginning of the each figure. This peak occurs when all of the particles in the system dropped to the piston floor, and because the simulation used spring force model, some of the particle bounced back; this creates a drop in the piston floor force. Therefore, a "spike" peak is expected for every simulation.

Another type of simulation was performed, which looked at the packing structures in a horizontal plane where it parallels to the x and z-plane. Mueller, did many extensive studies on the loose pack of spheres in cylinders [5~7]. In this thesis, most radial void fraction results were compared to Mueller's published data. This will provide further

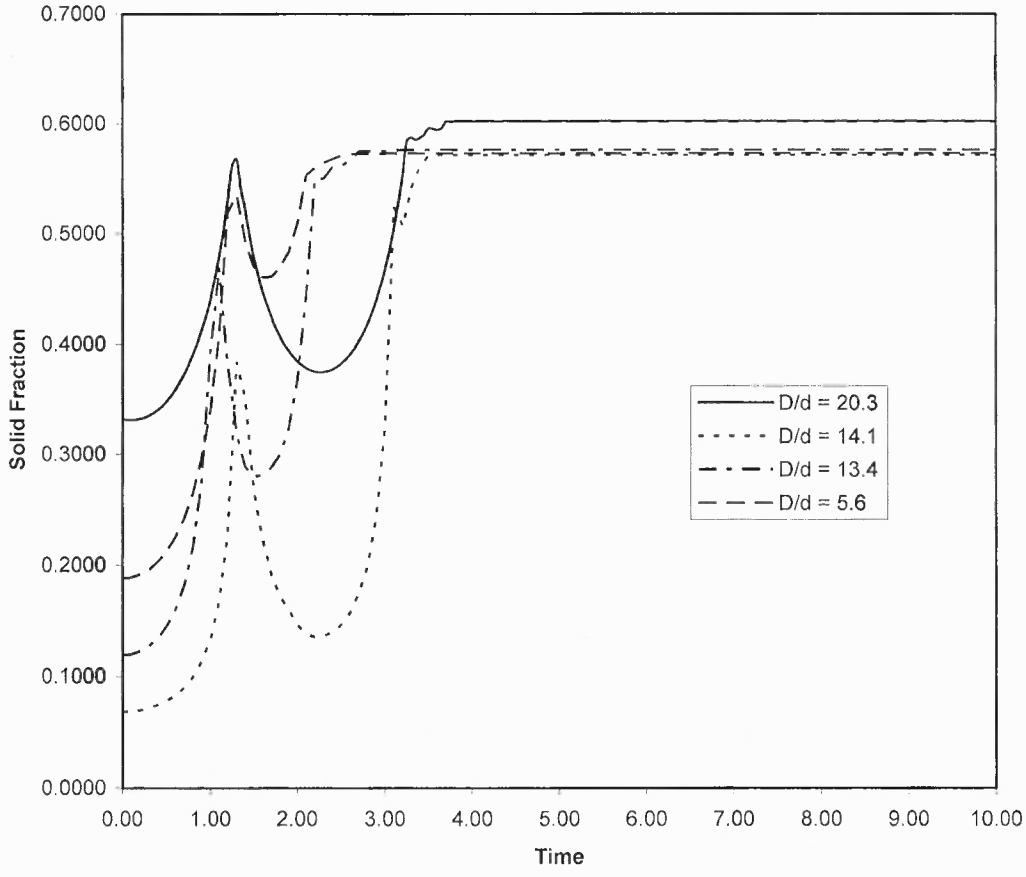

Figure 3.12 Solid fractions versus Time in different system configurations. The systems has fill height H/D = 5 with particle diameter of 1mm. The solid fraction results in these systems show a consistence of 0.6.

evidence of the accuracy and reliability of the partial volume calculation performed in this thesis.

The experimental and analytical data from Mueller [22] shows the accuracy of the packing of this DEM simulation. The radial void fraction is defined as the void volume divided by the total volume, and has been calculated for each diameter aspect ratio. The Figure 3.13 shows the radial void fraction for four diameter aspects ratios. The demands, triangles, circles, and the x are the DEM simulation results and the dashed lines are the experimental data from Mueller [22]. These simulated results show the

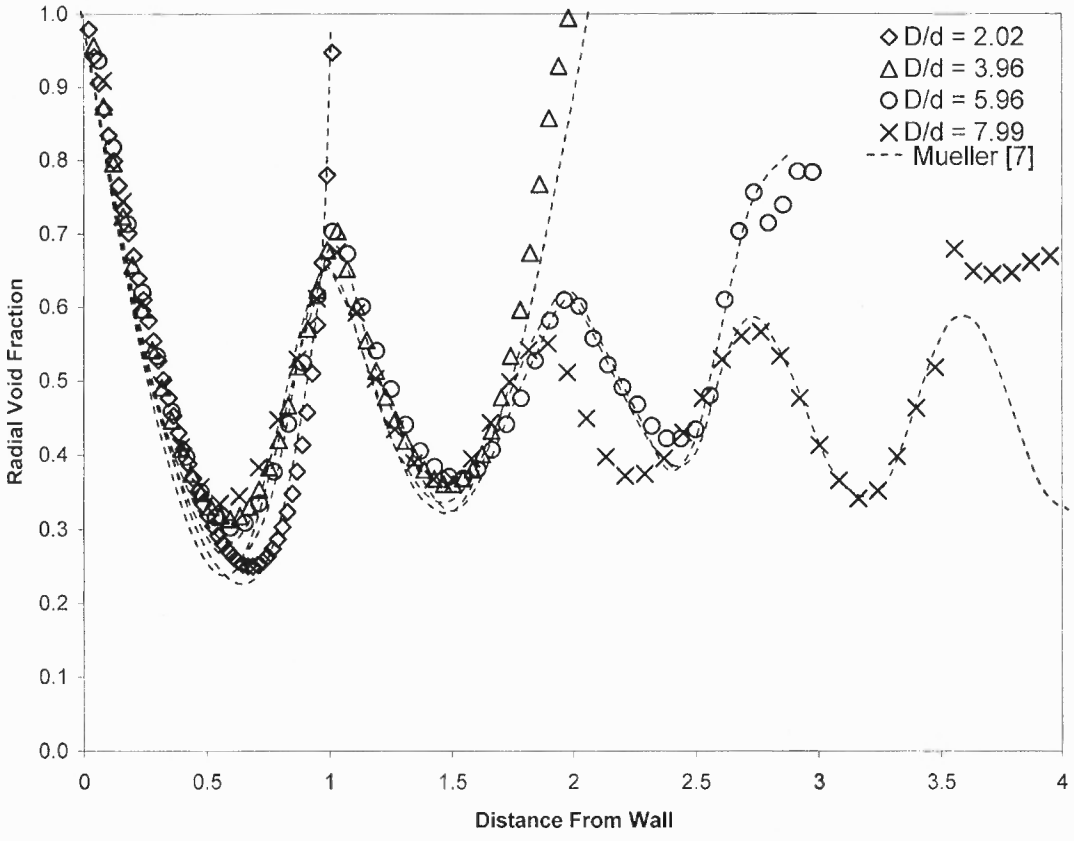

Figure 3.13 Radial void fraction comparisons between simulation and experimental data. There are four cases in these results and they are relatively small systems mainly because the compared data comes from an experimental data performed by Mueller.

packing algorithm can accurately simulate the static equilibrium positions for the loose packing of packed beds with D/d >2.0 [21].

However, in order to calculate the radial pressure, a bigger system is needed to be tested. Abreu and Castier [20] used the Monte Carlo method to simulate the packing and segregation of spheres in cylinders. Larger diameter aspects ratios for the sphere packing simulations were used and the results are comparable with the computational experiments done by Mueller.

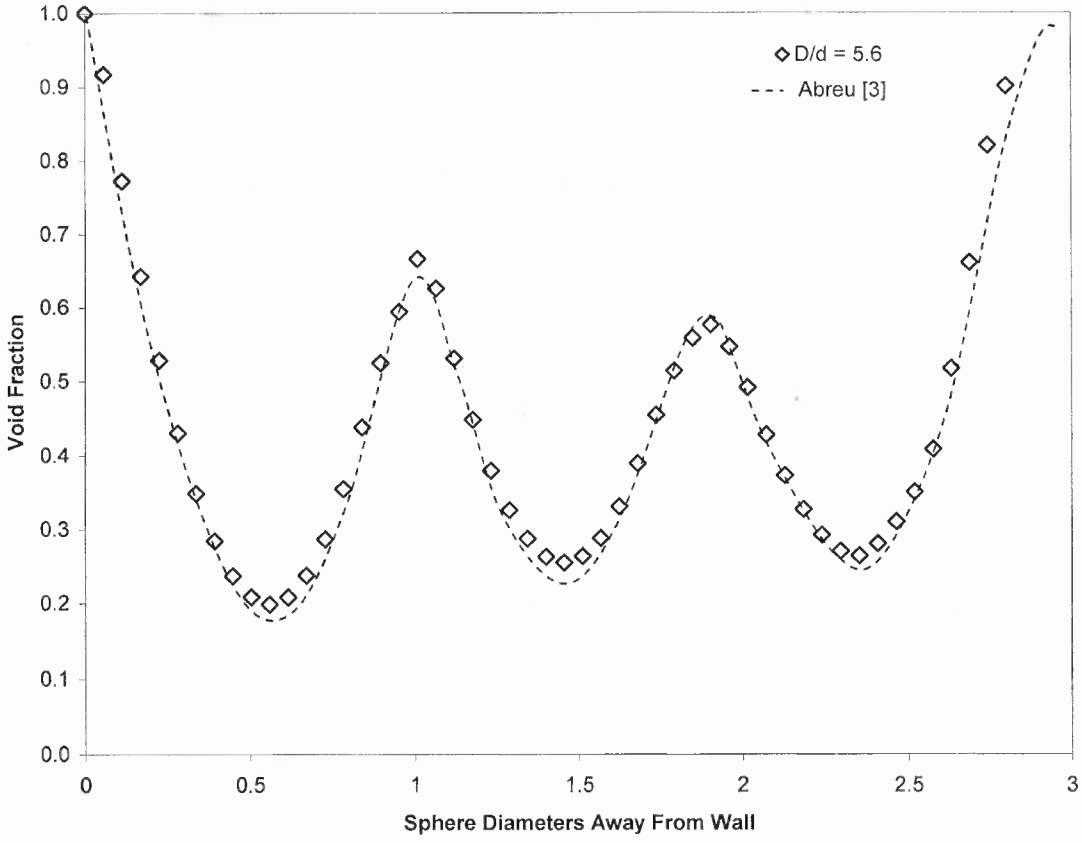

Figure 3.14 Radial void fraction profile in cylindrical packed beds with D/d = 5.6. The diamonds are the DEM simulation results and the dashed line is the Monte Carlo simulation performed by [20].

Figure 3.14 shows the data from the DEM simulation compare with the Monte Carlo simulation from [20]. The comparison clearly shows a great deal of similarity between the two simulations. Moreover, at diameter ratio D/d = 5.6, both the wall and the center of the cylinder have similar features, thus confirming that the wall effect translates throughout the cylinder vessel.

Figure 3.15 shows the comparison between the DEM simulation and Monte Carlo simulation in [20] with diameter ratio D/d = 14.1. The results from the DEM simulation is very similar compare to Figure 3.13 and 3.14 at the wall, however, the void fraction becomes unpredictable when close to the center of the cylinder. This is due to the loose

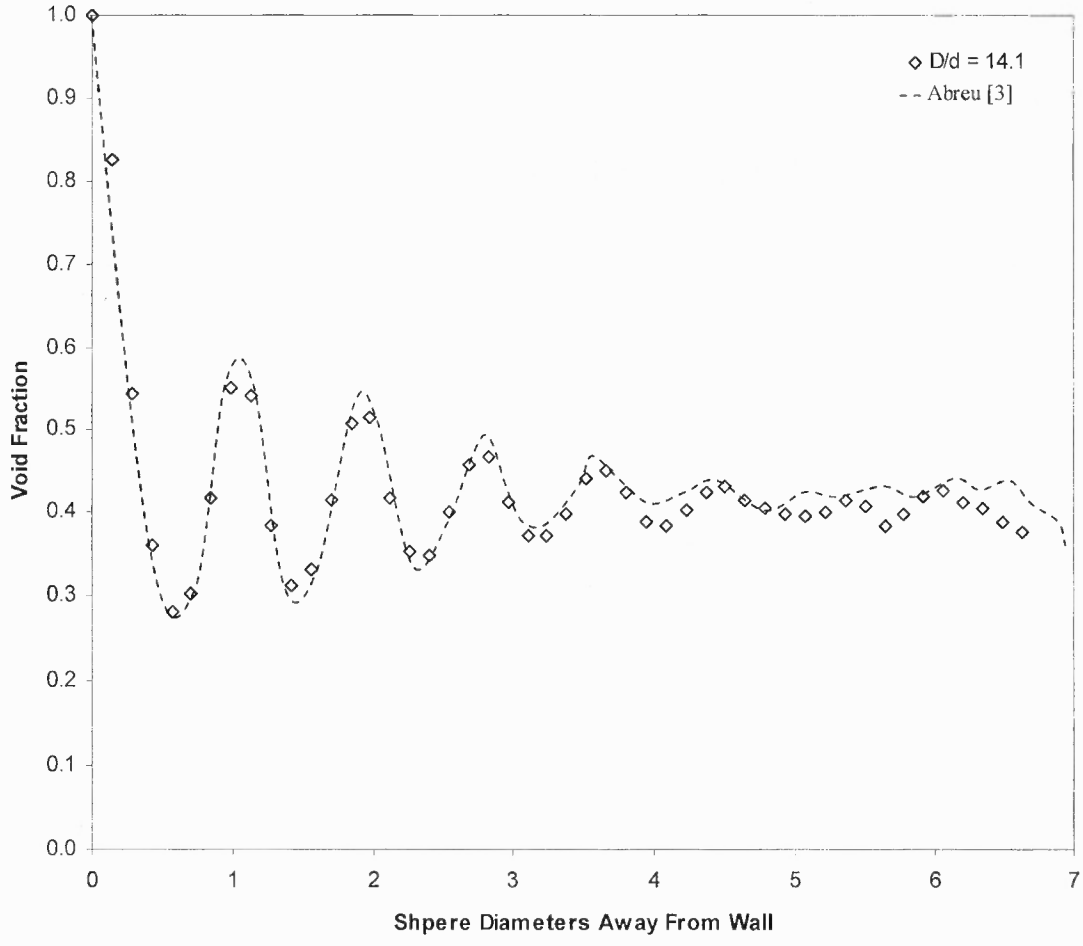

Figure 3.15 Radial void fraction profile in cylindrical packed beds with D/d = 14.1. The diamonds are the DEM simulation results and the dashed line is the Monte Carlo simulation performed by [20].

packing configuration of the system. As the diameter ratio increases, the wall effect only can be seen in the first few layers of the packing. However, as the layer of the packing increases, the wall effect is gone, the center of the packing becomes unpredictable.

Figure 3.16 below shows a comparison between DEM simulation and the Monte Carlo simulation results with diameter ratio D/d = 20.3. Figure 3.16 shows the results similar to those depicted in Figure 3.15. The wall effect only can be seen in the first few layers of the packing then decays towards the center of the cylinder.

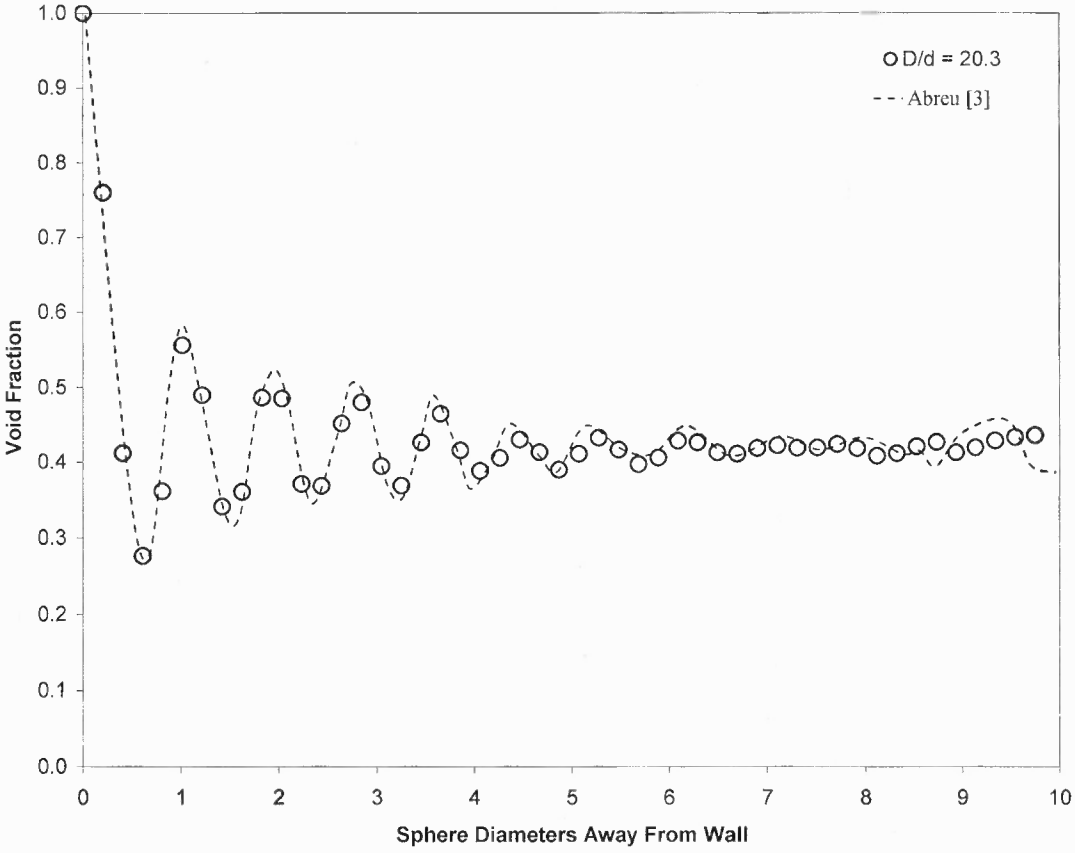

Figure 3.16 Radial void fraction profile in cylindrical packed beds with D/d = 20.3. The circles are the DEM simulation results and the dashed line is the Monte Carlo simulation performed by [20].

Overall the DEM simulation obtains comparable results to those from the experiments and the other simulations. When a smaller diameter ratio is present, the wall effect translates through out the cylinder vessel. However, as the diameter ratio increases, the structure of the particles near the lateral wall of the cylinder progressively decays towards the center of the cylinder. Therefore, the radial pressure is also has a relationship with the wall effect and the particle packing configuration. The next chapter will discuss the calculation of the radial pressure in the cylinder vessel, and also the relationship between the radial pressure and the normal pressure.

CHAPTER 4

SIMULATION RESULTS

The average radial pressure, <*Prr*>, and piston load, *F*, are computed by using DEM simulation. As stated in Chapter 2, the simulation randomly dumps particles into the cylinder, which is the cylinder user specified in the input file *i3ds*. Then, the particles start to move downwards by the gravitational force. The time when the piston floor of the cylinder starts moving thereby activating the frictional force on the cylinder wall is specified by the user. The speed of the piston floor is set to 0.001 diameters per second to ensure the velocity is small enough so that inertial effects are not important in the behavior of the system.

4.1 Static Simulation

Static simulations were performed to better understand the role wall friction plays in Jansen's theory. The static simulation shows that, as the fill height (H/D) increases, the force acting on the piston equals the weight of the particles in the system. This is due to the fact that the friction on the wall is not 'activated' by using the stationary piston. The simulation time was set to 120 seconds in order ensuring the particles in the system have reached their relaxed state. Table 4.1 below shows the simulation parameters used for the static simulation.

These static cases were computed at a diameter ratio H/D of 13.33 with particle diameter $d = 0.001$ meters, particle friction coefficient $\mu_p = 0.1$, and wall friction coefficient $\mu_w = 0.12$. A solids fraction ϕ of 0.6 was used in order to determine the number of particles,

Table 4.1 Parameters Used for Static Simulations.

Case	H/D	D/d	μ_w	μ_p	ϕ	np
1	0.187	13.33	0.12	0.1	0.6	399
2	0.375	13.33	0.12	0.1	0.6	799
3	0.75	13.33	0.12	0.1	0.6	1599
4	1.125	13.33	0.12	0.1	0.6	2398
5	1.5	13.33	0.12	0.1	0.6	3198
6	1.875	13.33	0.12	0.1	0.6	3997
7	2.25	13.33	0.12	0.1	0.6	4796
8	2.812	13.33	0.12	0.1	0.6	5994
9	3.374	13.33	0.12	0.1	0.6	7192

np, in the systems, according to the following formula:

$$np = \frac{3}{2}\left(\frac{D}{d}\right)^3\left(\frac{H}{D}\right)\phi \tag{4.1}$$

The results of the simulations are shown in Figure 4.1 and Figure 4.2 below.

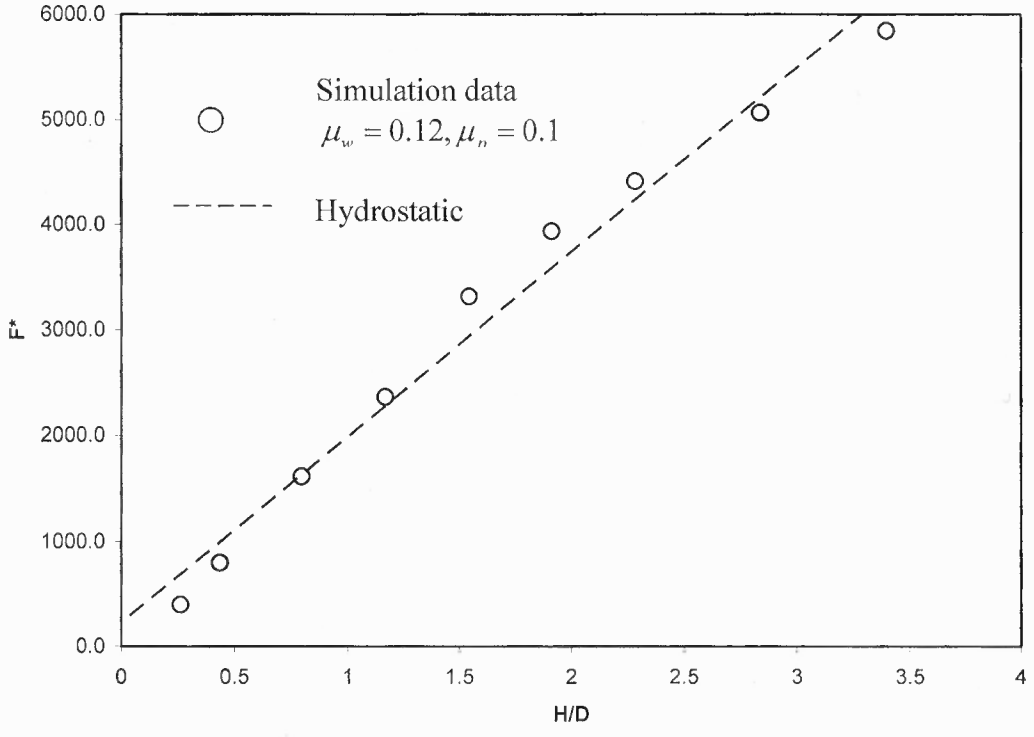

Figure 4.1 Static simulations for piston load. Simulated data with wall friction coefficient of 0.12 and particle friction coefficient of 0.1. The circle is the results from DEM simulation and the dashed line is the Hydrostatic curve.

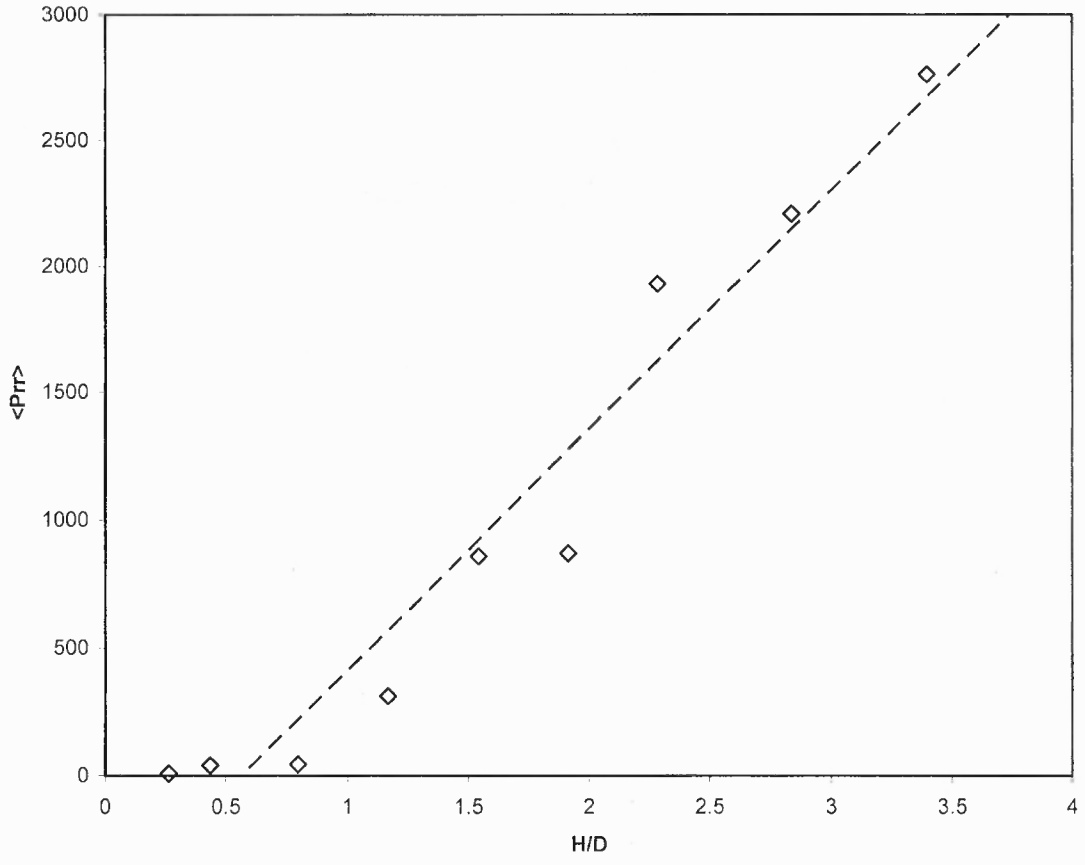

Figure 4.2 Static Simulations for the average radial pressure of the cylinder. The dished line here is the trend line for better visual.

Figure 4.1 contains the force on the piston versus the fill height (H/D) and the piston load shows hydrostatic behavior. The observed force showed some slight deviation from linearity duo to the presents of frictional forces between the particles as well as the fact that this system has a loose packing configuration.

Figure 4.2 contains the average radial pressure of the whole cylinder versus the fill height (H/D) and the average radial pressure shows hydrostatic behavior in the static simulations. Moreover, as the fill height (H/D) increases, the average radial pressure (<Prr>) increases.

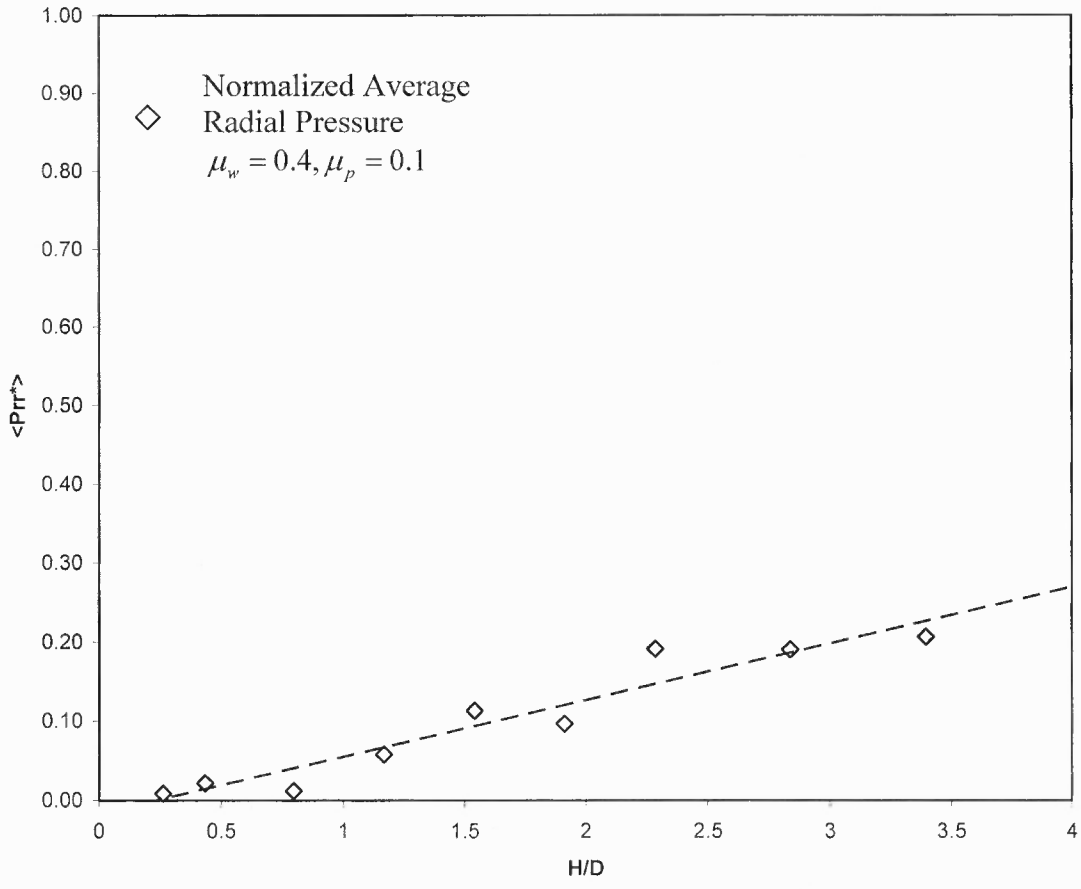

Figure 4.3 Static simulations for normalized average radial pressure. The dished line represents the trend line for better visual.

Figure 4.3 below shows the normalized average radial pressure versus the fill height, H/D. Since the average radial pressure is being normalized by dividing by the normal pressure on the piston, Figure 4.3 clearly shows the normal pressure is much higher than the average radial pressure. This is due to the fact that the cylinder does not have wall friction and, therefore, has smaller average radial pressure.

Overall the static simulation results show that as the fill height H/D increases, the average radial pressure increases as well. This phenomenon is expected, since more particles are introduced into the system and create more pressure on the lower layers of

the particles as fill height increases. This can be explained by the bottom piston load as well; as more weight is introduced into the top layer, the load on the piston increases as much as the weight that has been added. These static simulations clearly show that the piston load and average radial pressure depend largely on the values of the fill height H/D. However, Janssen's theory is in the form of a dynamic system where friction is activated. In Chester [6], he suggested that in order to eliminate the hydrostatic behavioral region, wall friction must be activated. Furthermore, Chester also suggested that to have particles contact wall with friction, there must be a motion in the system relative to the cylinder.

4.2 Dynamic Simulations

4.2.1 Overview

Dynamic simulations were performed in order to study the effect of wall friction in these granular systems; the parameters of these simulations are shown in Table 4.2. These dynamic cases were performed with a piston which was translated downwards in the negative y-direction. The velocity of the piston is suggested by Chester which $v_p = 0.001$ diameters per second [6]; this piston velocity is small enough so that inertial effects are not important in the behavior of the system.

The results in this section are divided into three parts; part 1 corresponds to the cases shown in Chapter 3 where the calculations are determined by the whole cylinder. The second part of this section contains the cases determined by horizontal cross section of the cylinder and the last part consists of the cases determined by the vertical cross section of the cylinder.

Table 4.2 Parameters used for Dynamic Simulations.

Case	H/D	D/d	μ_w	μ_p	ϕ	np
1	0.187	13.33	0.12	0.1	0.6	399
2	0.375	13.33	0.12	0.1	0.6	799
3	0.75	13.33	0.12	0.1	0.6	1599
4	1.125	13.33	0.12	0.1	0.6	2398
5	1.5	13.33	0.12	0.1	0.6	3198
6	1.875	13.33	0.12	0.1	0.6	3997
7	2.25	13.33	0.12	0.1	0.6	4796
8	2.812	13.33	0.12	0.1	0.6	5994
9	3.374	13.33	0.12	0.1	0.6	7192
10	4.049	13.33	0.12	0.1	0.6	8631
11	4.859	13.33	0.12	0.1	0.6	10358
12	5.831	13.33	0.12	0.1	0.6	12430
13	6.997	13.33	0.12	0.1	0.6	14916
14	8.3964	13.33	0.12	0.1	0.6	17899
15	10.076	13.33	0.12	0.1	0.6	21479
16	0.187	13.33	0.4	0.1	0.6	399
17	0.375	13.33	0.4	0.1	0.6	799
18	0.75	13.33	0.4	0.1	0.6	1599
19	1.125	13.33	0.4	0.1	0.6	2398
20	1.5	13.33	0.4	0.1	0.6	3198
21	1.875	13.33	0.4	0.1	0.6	3997
22	2.25	13.33	0.4	0.1	0.6	4796
23	2.812	13.33	0.4	0.1	0.6	5994
24	3.374	13.33	0.4	0.1	0.6	7192
25	4.049	13.33	0.4	0.1	0.6	8631
26	4.859	13.33	0.4	0.1	0.6	10358
27	5.831	13.33	0.4	0.1	0.6	12430
28	6.997	13.33	0.4	0.1	0.6	14916
29	8.3964	13.33	0.4	0.1	0.6	17899
30	10.076	13.33	0.4	0.1	0.6	21479
31	0.187	13.33	0.8	0.1	0.6	399
32	0.375	13.33	0.8	0.1	0.6	799
33	0.75	13.33	0.8	0.1	0.6	1599
34	1.125	13.33	0.8	0.1	0.6	2398
35	1.5	13.33	0.8	0.1	0.6	3198
36	1.875	13.33	0.8	0.1	0.6	3997
37	2.25	13.33	0.8	0.1	0.6	4796
38	2.812	13.33	0.8	0.1	0.6	5994
39	3.374	13.33	0.8	0.1	0.6	7192
40	4.049	13.33	0.8	0.1	0.6	8631
41	4.859	13.33	0.8	0.1	0.6	10358
42	5.831	13.33	0.8	0.1	0.6	12430
43	6.997	13.33	0.8	0.1	0.6	14916
44	8.3964	13.33	0.8	0.1	0.6	17899
45	10.076	13.33	0.8	0.1	0.6	21479

In cases 1 – 15, the wall friction coefficients μ_w were set to 0.12 and the particle friction coefficients μ_p were set to 0.1. In cases 16 – 30, the wall friction coefficients μ_w were set to 0.4 and the particle friction coefficients μ_p were set to 0.1. Lastly, in cases 31 – 45, the wall friction coefficients μ_w were set to 0.8 and the particle friction coefficients μ_p were set to 0.1. The simulation time for these dynamic cases was set to 320 seconds, except cases 13 – 15, 27 – 30 and 42 – 45 were set to 460 seconds to make sure the average radial pressure and force on the piston were in the relaxation state. All of the dynamic cases have the diameter ratio D/d set to 13.33 and the piston was moved downwards to activate the wall friction.

4.4.2 Results for the Whole Cylinder

The results for the whole cylinder are described in this section. The piston force is being studied here to confirm the behavior predicted by Janssen's model where $F^*(H/D) = \frac{1.5\nu(D/d)^3}{\lambda}\left(1-e^{-\lambda(H/D)}\right)$. In the Janssen's prediction, the F^* is a dimensionless force and $\lambda = 4\mu\frac{1-\sin\left(\tan^{-1}\mu\right)}{1+\sin\left(\tan^{-1}\mu\right)}$. In order to calculate this dimensionless force, the piston force F_z is being normalized by a single particle weight and therefore $F^* \equiv \frac{6F_z}{\rho g \pi d^3}$

The results shown in the Figure 4.4 below are extended, from H/D = 2.4 to H/D = 10.076, from those in [6]. The circles, diamonds and x are the simulated data from cases 1-15, 16 – 30 and 31 – 45 respectively. The dashed lines and the solid line are the

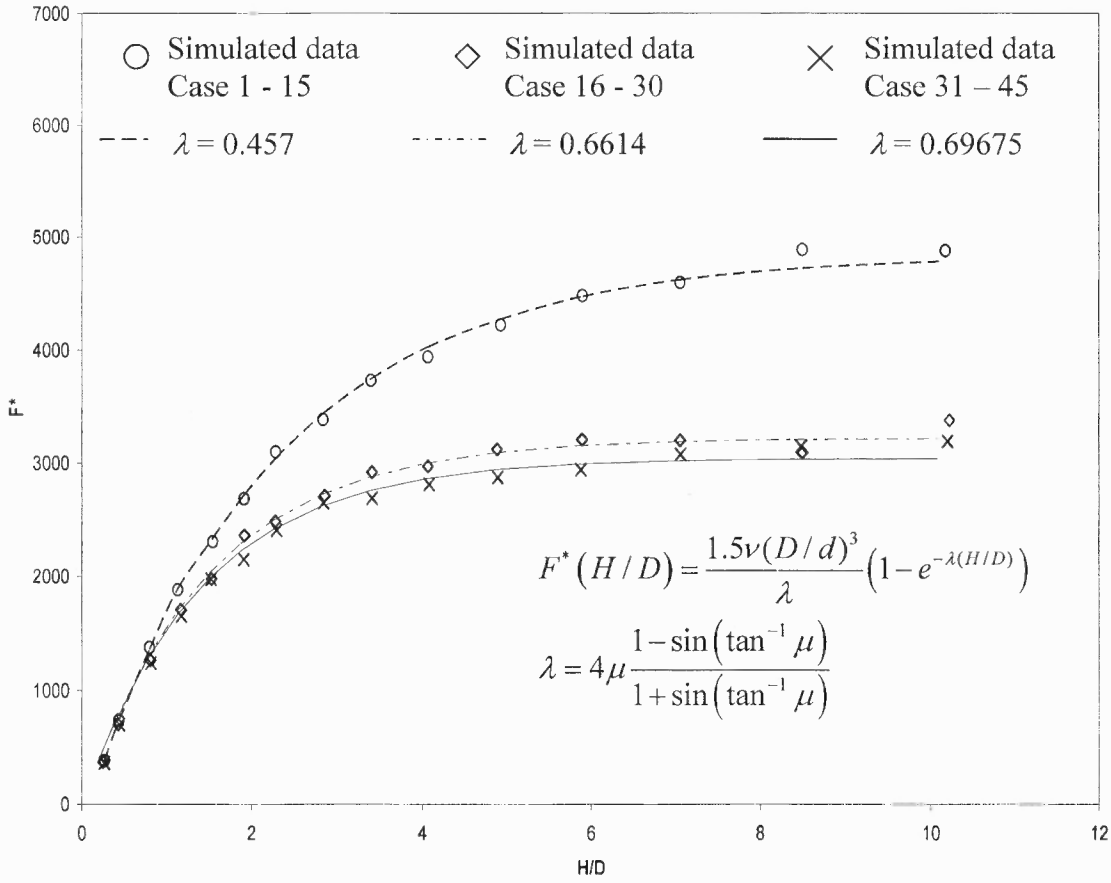

Figure 4.4 Dynamic simulation for piston load for case 1-45. Case 1-15 has wall friction of 0.12, Case 16-30 has wall friction of 0.4 and Case 31-45 has wall friction of 0.8.

Janssen's prediction of normal force; in this case, the piston force versus fill height H/D. In these simulations, the wall friction coefficient was set to 0.12, 0.4, and 0.8 with the particle friction coefficient 0.1. The diameter ratio D/d was 13.33 for all of the cases. The results show a clear fit with Janssen's theory. The simulation in these cases was run until the piston force reached its relaxation state. However, with the higher fill height, the time for the particles to reach their relaxation state increase from 320 seconds to 420 seconds.

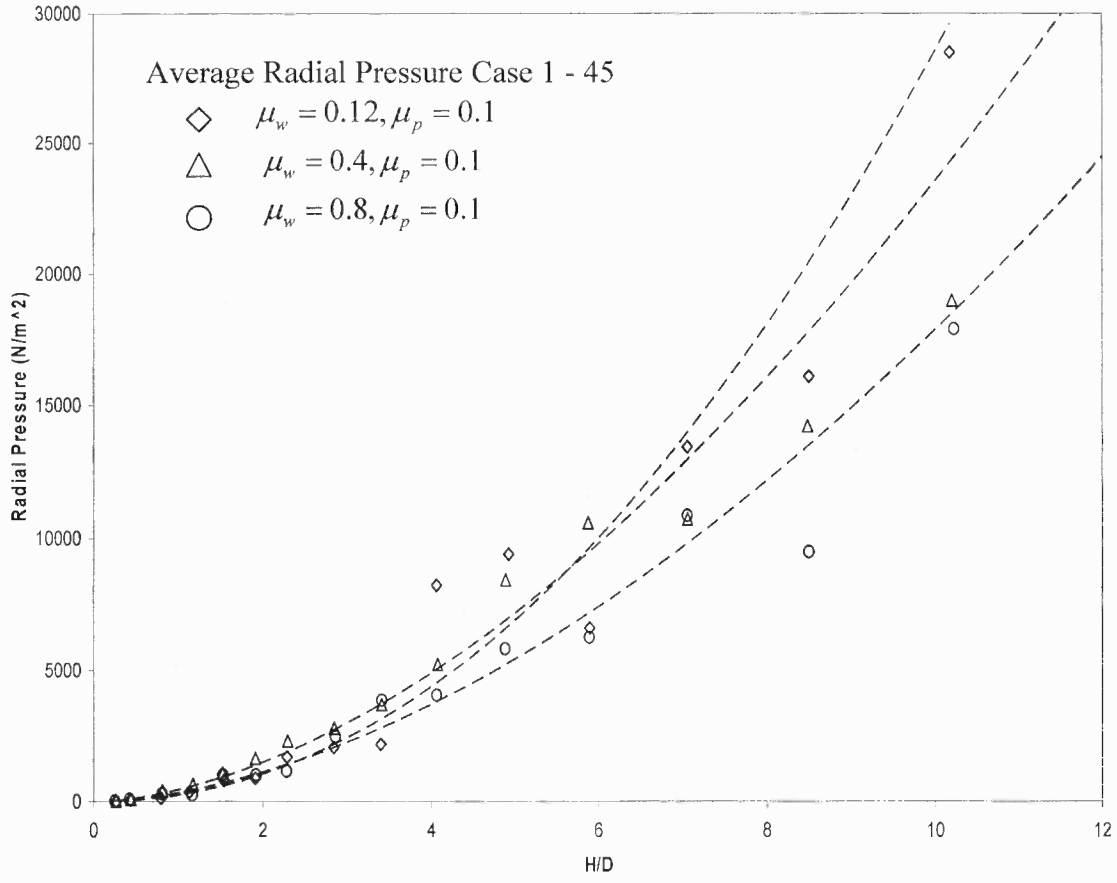

Figure 4.5 Dynamic simulation for radial pressure for case 1 – 45. The diamonds, triangles and circles represent the cases with wall coefficients friction equals to 0.12, 0.4 and 0.8 respectively. The dashed lines are the trend line for better visual.

The average radial pressure results shown in Figure 4.5 below demonstrate that as the fill heights (H/D) increases, the average radial pressure increases. Clearly, these results cannot alone describe the behavior of the average radial pressure in a system. Therefore, more study were performed to better understand this matter.

The average radial pressure and normal pressure in Figure 4.6 are normalized by the equilibrium value of the normal pressure in Figure 4.4. For example, in the case where the wall coefficient of friction equals to 0.12, one can pick a value from the normal pressure where the dashed line become equilibrium; then the average radial pressure and

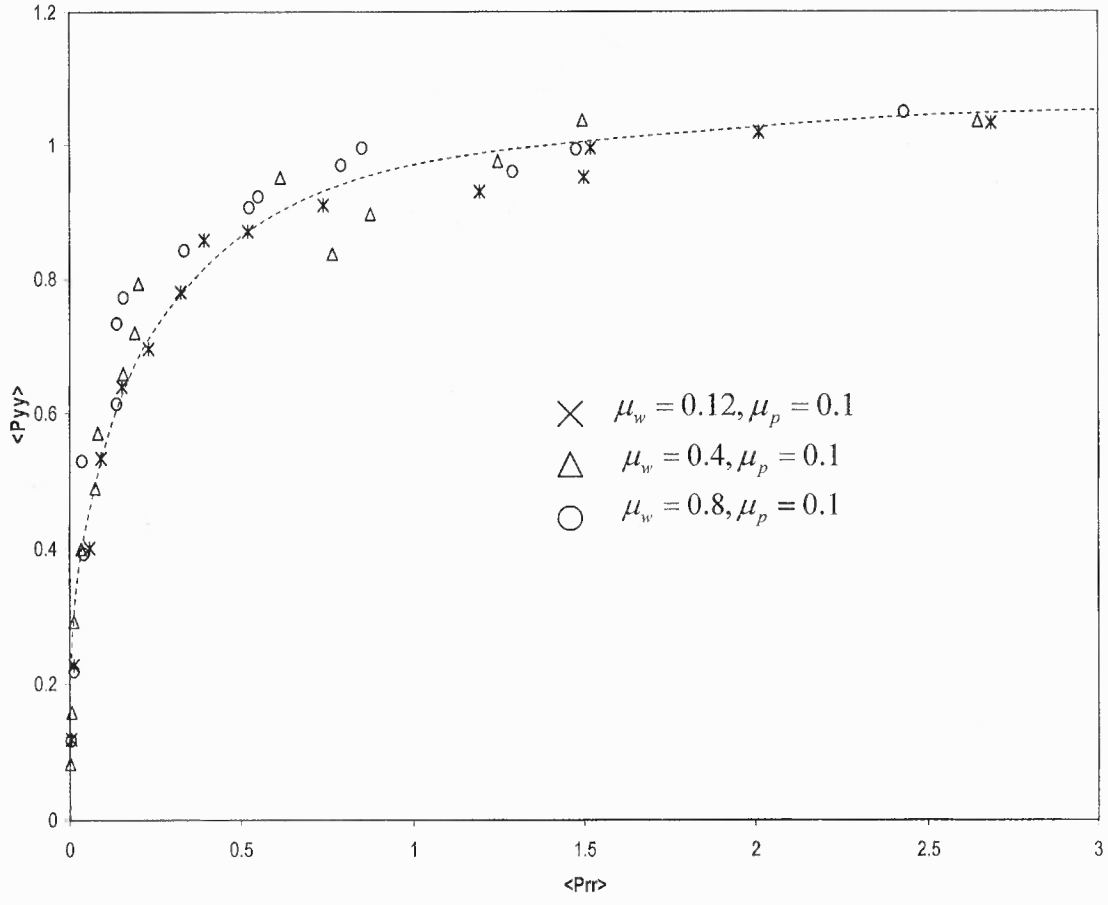

Figure 4.6 Normalized average radial pressure and normalized normal pressure. The x, triangles and circles represent the cases with wall coefficients friction equals to 0.12, 0.4 and 0.8 respectively. The dashed line is the trend line for better visual.

the normal pressure are divided by this number. These cases show a similar behavior as was observed in piston force versus fill height (H/D). The results of normal pressure versus average radial pressure show that as the normal pressure increases, the average radial pressure increases. However, when normal pressure becomes equilibrated as the fill height increases, the average radial pressure is still increasing. These results violate Janssen's assumption that the lateral stress is a fixed fraction of the axial stress.

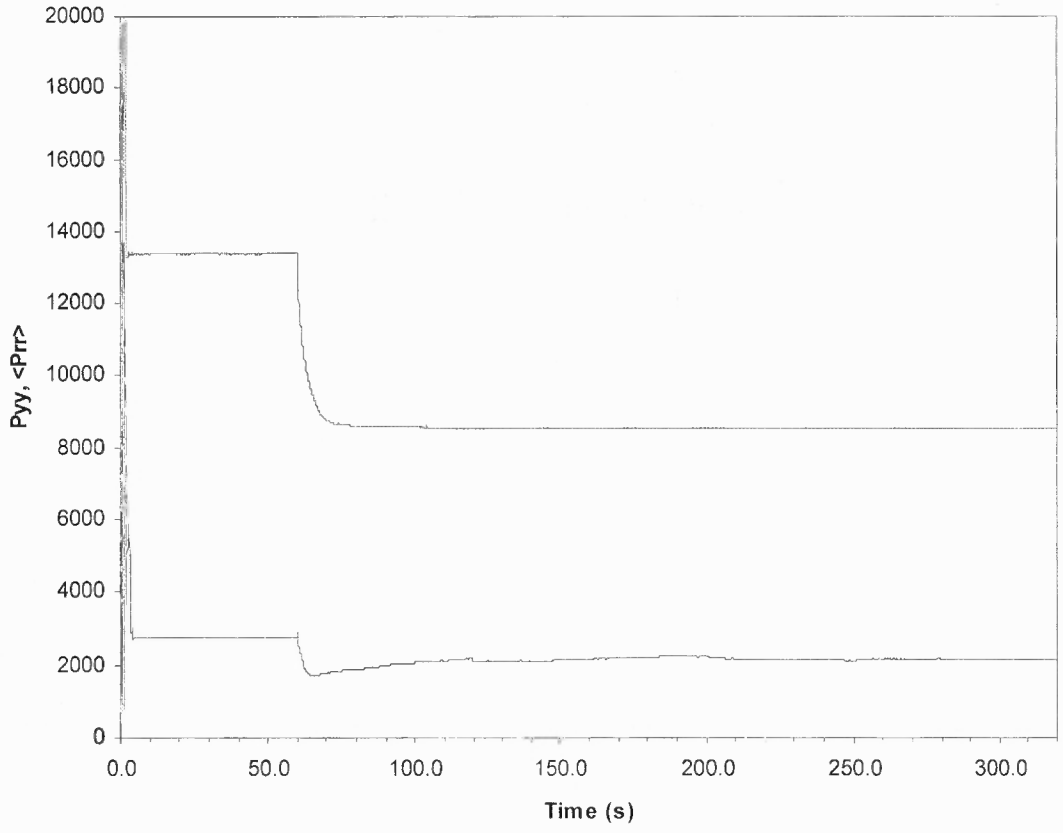

Figure 4.7 Time revolution of normal pressure, Pyy, as solid line and average radial pressure, <Prr>, as dashed line, in one simulation case.

In order to understand the results of the average radial pressure, more investigations were completed. In the Figure 4.7, the total simulation time is 320 seconds, and at time equals 60 seconds, the piston floor starts to move downwards and the normal and average radial Pressure start to decrease. The reason for the relaxation time between the initial time and the time the piston starts to move is to ensure that all the particles have reached relaxation state even for the systems with higher fill heights.

The results from this thesis are all post processed by using "Time Averaging". The time averaging method selects a set of times where kinetic energy of the system has become zero and then averages the resultant values at these times to get the final results.

Figure 4.6 shows both normal pressure, *Pyy*, and average radial pressure, <Prr>, become constant around 260 to 270 seconds. The last 20 seconds of data are then averaged. However, the graph shows the average radial pressure took a longer time to reach its relaxation than the normal pressure as the piston moves. The normal pressure becomes constant almost immediately after the piston itself starts to move; around 5 seconds, as shown in Figure 4.7. However, the average radial pressure still had not shown any sign of becoming constant by this time. This is expected because the average radial pressure mostly depends on the packing configuration of the system. When the piston floor starts to move down, the lower layer of the particles starts to lose its packing configuration, and the loss of packing configuration will begin to propagate to the top layer. This can be seen in Figure 4.7 where the average radial pressure starts to decrease as the piston starts to move down, and as soon as the propagation stops, (note the piston still moves down), the radial pressure starts to increase. The increase in the average radial pressure occurs because all of the particles are trying to reconfigure themselves into a new packing configuration. As these particles try to repack, the interaction between the particles and the cylindrical wall increases, thus increasing the average radial pressure.

Figure 4.8 below shows the evolution of the average radial pressure. The system reaches relaxation at different time depending on the fill height. With fill height H/D = 0.809, the average radial pressure <Prr> reaches relaxation much faster. As mentioned before, the velocity of the piston is 0.001 diameters per second and therefore, from Figure 4.8, the distance estimated that the piston moved for the average radial pressure to reach relaxation is 0.002 diameters in the case of H/D = 0.809. Therefore, for H/D = 1.5 and 2.812, the piston moved a distance of 0.165 and 0.24 respectively. As Figure 4.8 shows,

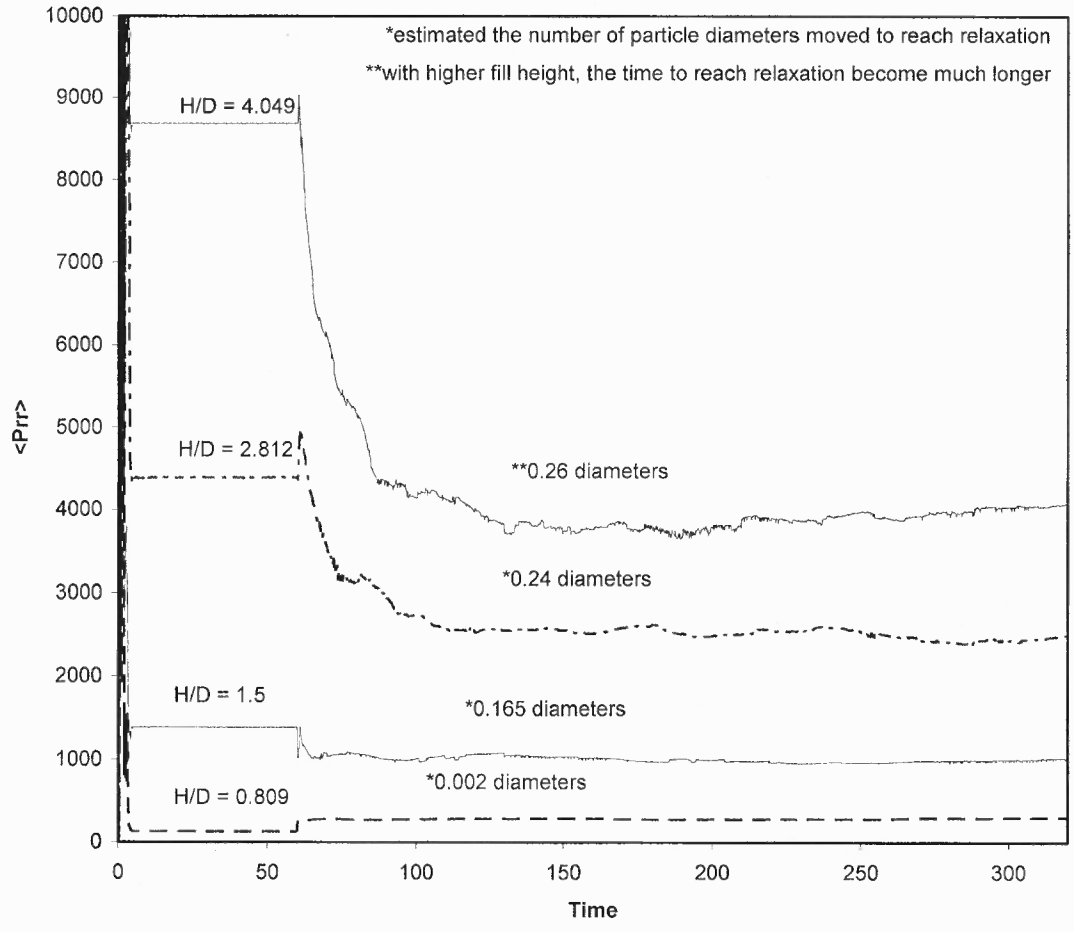

Figure 4.8 Average radial pressure <Prr> versus time with lower fill heights (H/D). The simulation time needed for average radial pressure to reach relaxation becomes longer as fill heights increases.

at H/D = 4.049, the time required for the average radial pressure to reach relaxation was greater while, at the end of the simulation, the average radial pressure had not yet reached equilibrium.

Figure 4.9 below contains results for fill heights much higher than in Figure 4.8; the simulation time also needed to be increased from 320 to 420 seconds here since the time for average radial pressure to reach relaxation increases. However, Figure 4.9

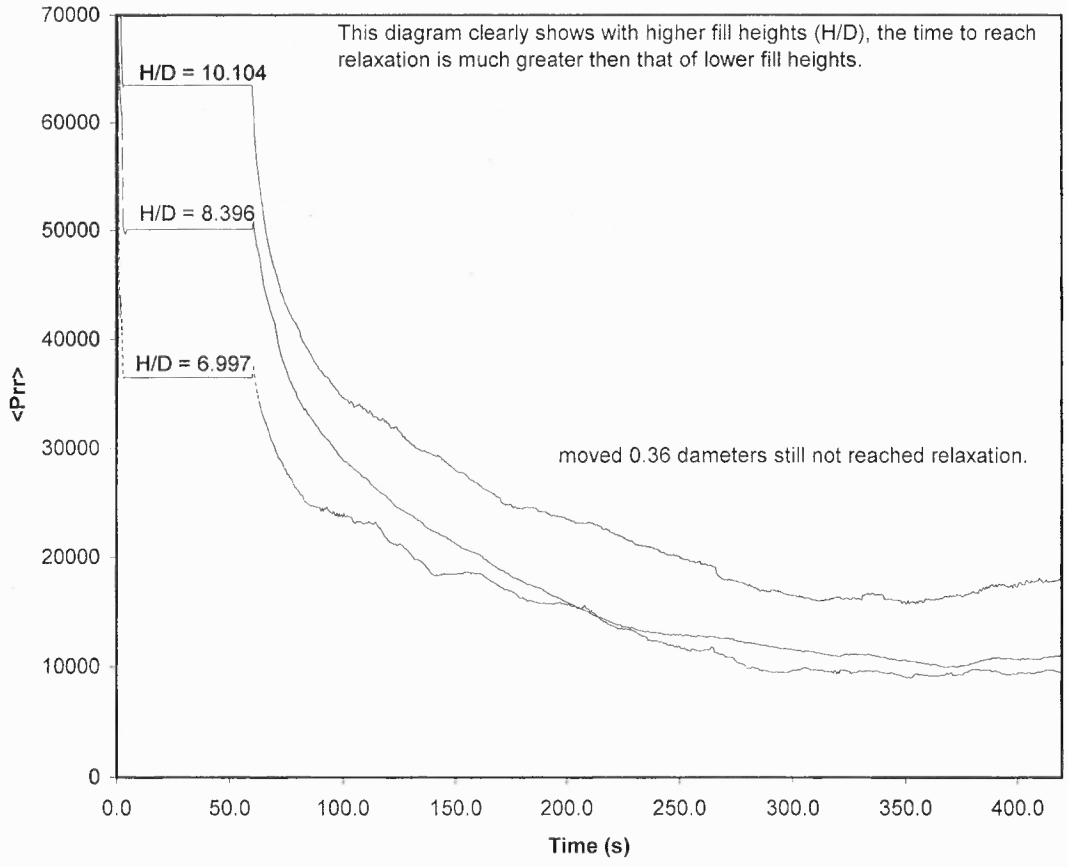

Figure 4.9 Average radial pressure <Prr> versus time with much higher fill heights (H/D). As the fill heights increases, the time for average radial pressure to reach relaxation increases.

shows that with H/D = 6.997 and 8.396, the average radial pressure is very close to becoming relaxed at the end of the simulation time, around 400 seconds.

4.2.3 Results for the Average Radial Pressure in Horizontal Cross Section Layers

The results from Figure 4.8 and Figure 4.9 show that the average radial pressure has fluctuations throughout the entire simulation time. Therefore, the average radial pressure in the horizontal cross section layers of the cylinder should be studied to better understand the vertical dependence of the average radial pressure.

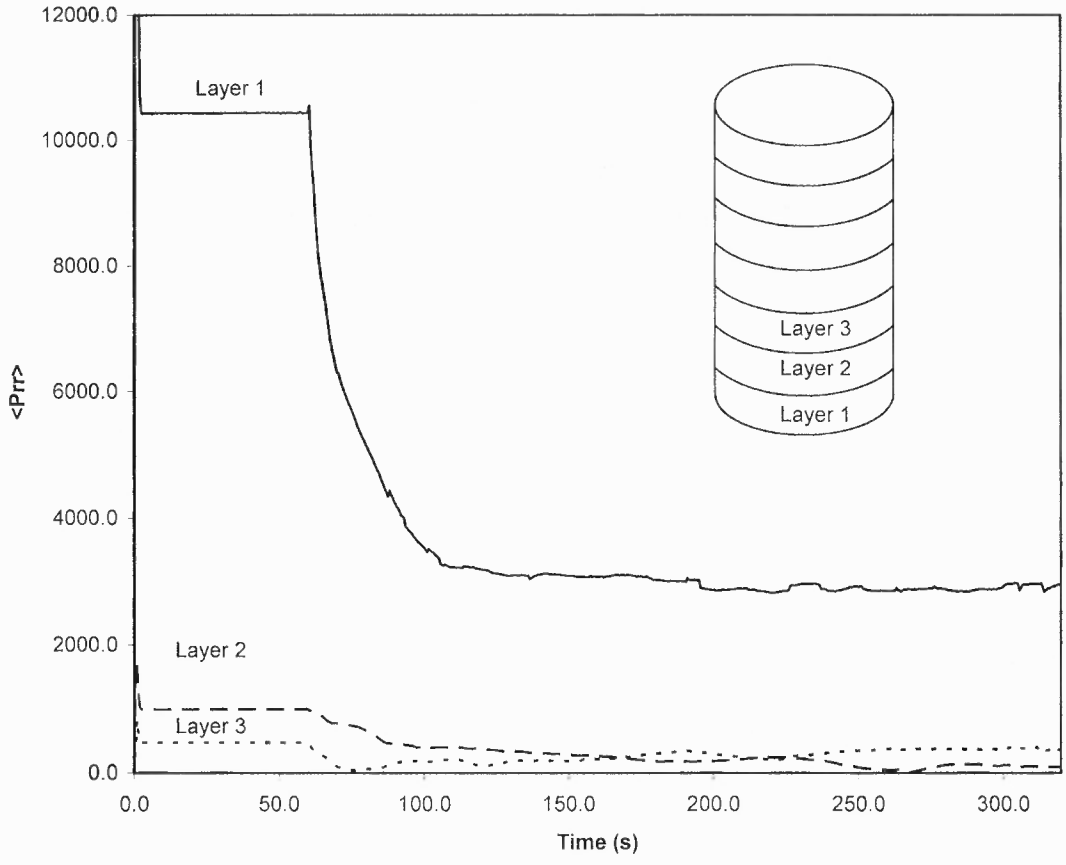

Figure 4.10 Average radial pressure in different layers of the cylinder. The Layer 1 represents the bottom floor piston and Layer 2, Layer 3 are each three diameters up from their lower layer. Each layers is 4 particle diameters height.

Figure 4.10 shows the results from simulation in where the cylinder was divided into 15 horizontal layers with each layer having a height of 4 particle diameters. The average radial pressure in the lower layers of the cylinder are much predictable, compared with Figure 4.8 and 4.9. The fluctuations are caused by the repacking of the particles when the piston moved. However, these fluctuations are small because the weight on top of the lower layers makes these particles reconfigure themselves faster.

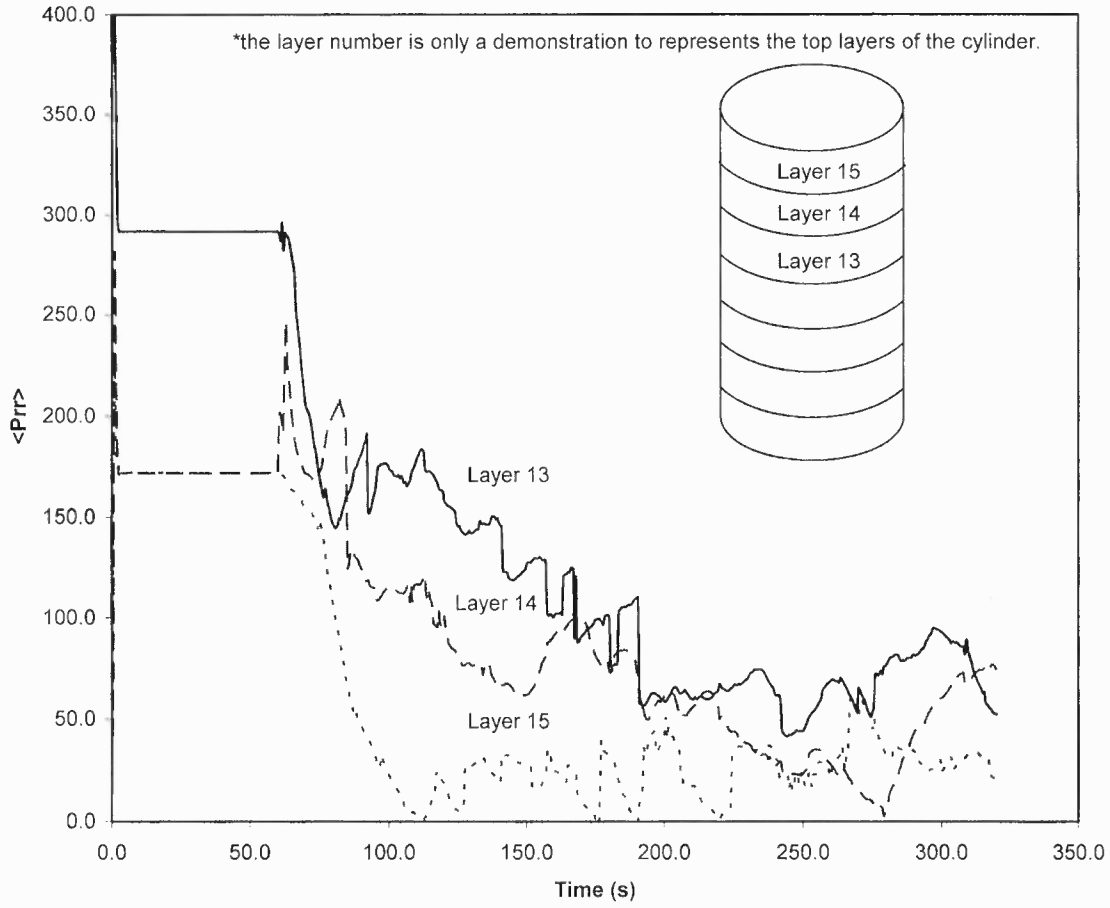

Figure 4.11 Average radial pressure in the top layers of the cylinder. Layer 15 represents the top fill height of the particles.

Figure 4.11 shows that, at the top layers of the cylinder, the average radial pressure has a large amount of fluctuation; over time the average radial pressure can not be identified. These fluctuations are caused by the particles constantly reconfiguring themselves; there is no weight on top of them to stop the reconfiguration process. Also notice that the average radial pressure in the top layers is much smaller than that in the lower layers. This is because the bottom layers have a greater weight on top of them and therefore have a larger radial pressure than the top layers of the cylinder.

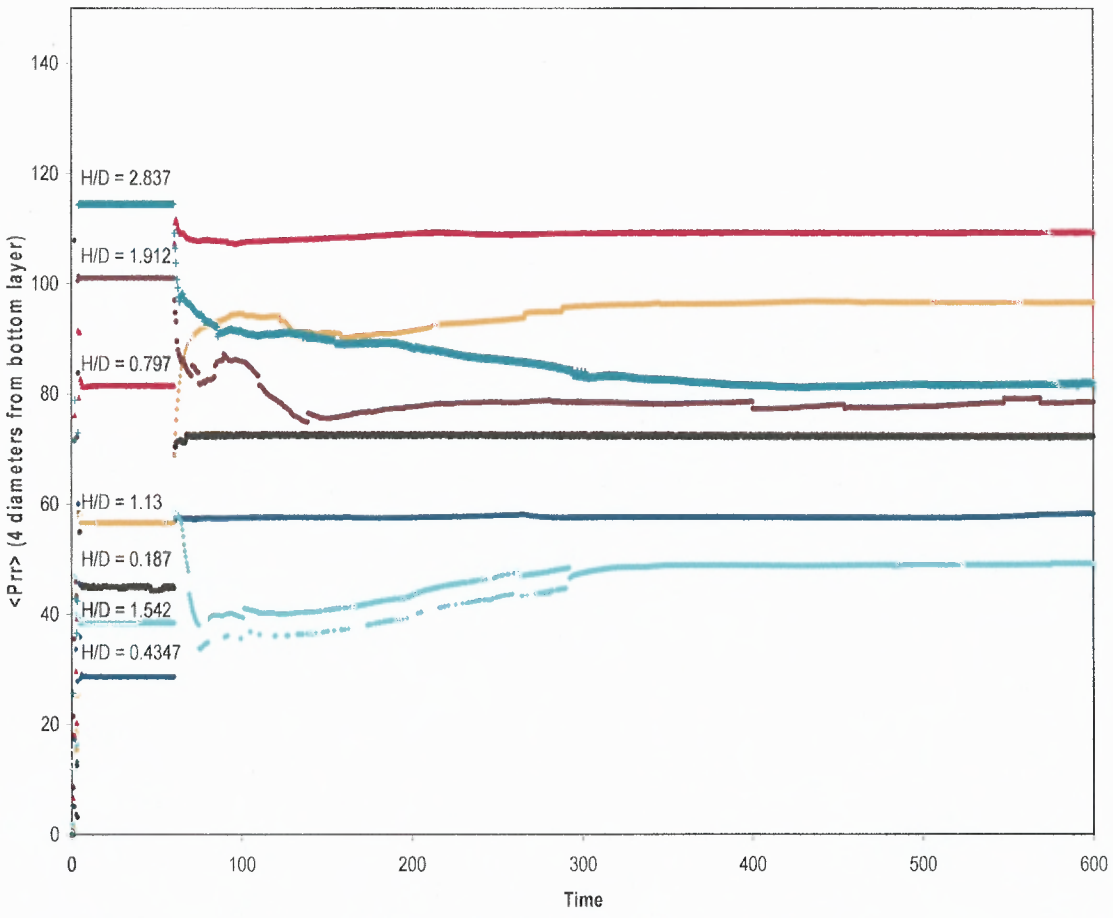

Figure 4.12 Average radial pressure in 4 diameters from bottom layer of the cylinder with different fill height (H/D).

From the results in Figure 4.10 and Figure 4.11, the average radial pressure results on the bottom layers of a cylinder have fewer fluctuations then the top layers. Therefore, the bottom layer of four diameters height in a cylinder is investigated.

The results from Figure 4.12 shows the average radial pressure in 4 diameters from bottom layer of the cylinder for systems with variations in fill height. The results show inconsistencies in average radial pressure with increases in the fill height. The author believes that since the packing configuration for these cases is loose packed configuration, the bottom layers of the particle could pack very differently at different fill

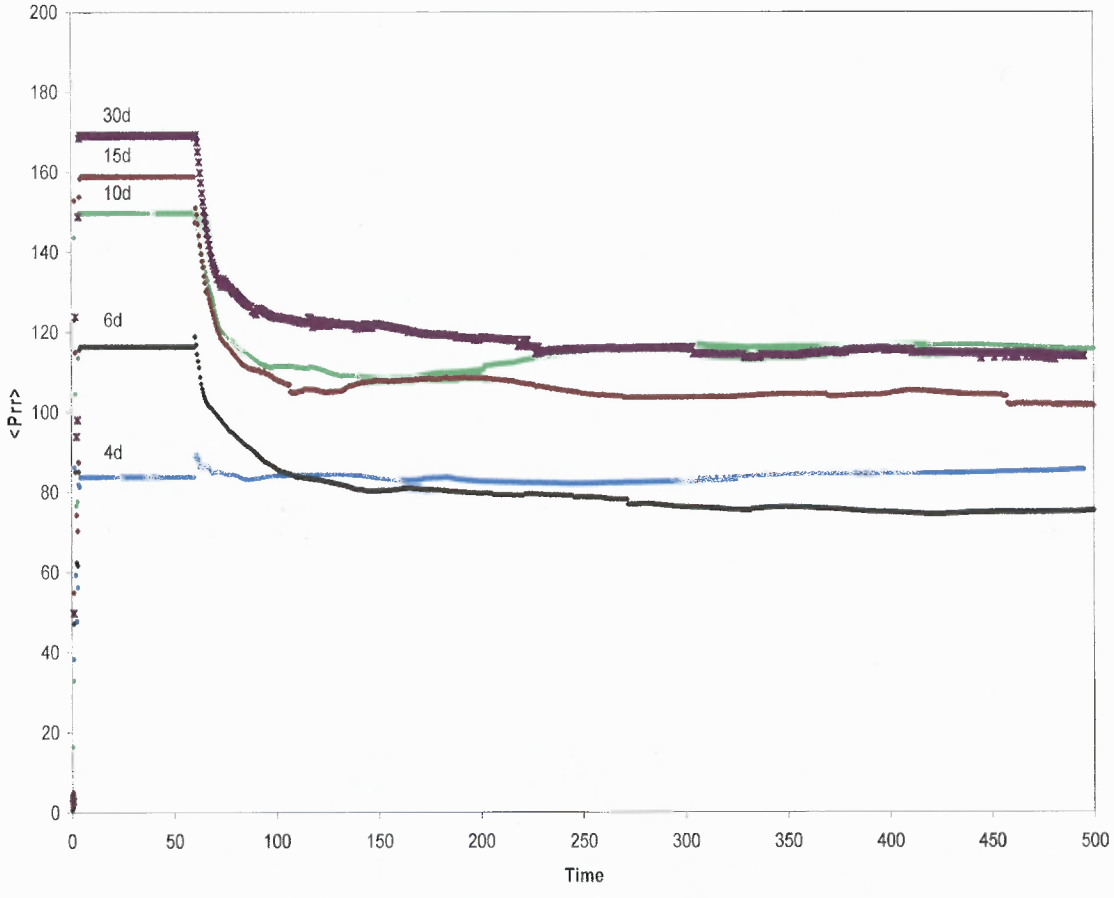

Figure 4.13 Average radial pressure as a function of the thickness (in particle diameters) of the control volume.

heights. Since the average radial pressure has high dependency on the configuration of the particles, the inconsistencies in the results in Figure 4.12 were caused by the packing configuration of the particles.

One more horizontal cross section layers analysis was conducted to further investigate the average radial pressure. Figure 4.13 shows the average radial pressure as a function of the thickness, in particle diameters, of the control volume. The thickness of the control volume ranges from 4 to 30 particle diameters. The results show that as the control volume thickness increases, the average radial pressure has different values. The relationship between the average radial pressure and the thickness is not understood;

however, the author believes this behavior may be related to the creation and destruction of force chains that have been reported in the literature [4, 16]. This result is in contrast to the behavior of the radial pressure versus the fill height; as the fill height increases the average radial pressure increases as shown in Figure 4.5.

4.2.4 Results for the Average Radial Pressure in Vertical Cross Section Layers

The average radial pressure within vertical cross section layers of the cylinder has been computed in order to understand the behaviors observed from section 4.2.3. These simulations were performed with the cylinder being sliced into numbers of symmetrical vertical cross section layers, with the fill height fixed.

Figure 4.14 below shows that the average radial pressure at the center of the cylinder is nearly zero, and as it gets close to the wall, the average radial pressure increases. This is mainly due to the forces from the weight being translated into the radial force as a result of the reconfiguration of the particles. Notice that the average radial pressure here is a *differential* pressure; in other words the average radial pressure calculated here is for each different R/d. As a check of the simulation results, using $\int P_{rr} d(R/d) = \langle P_{rr} \rangle$, one can estimate the total average radial pressure of the cylinder to be around 3191.3 N/m^2; in the simulation the pressure at the wall is 2785.2 N/m^2. This shows that the pressure between the particle-wall contact is much higher then the pressure in the particle-particle contact.

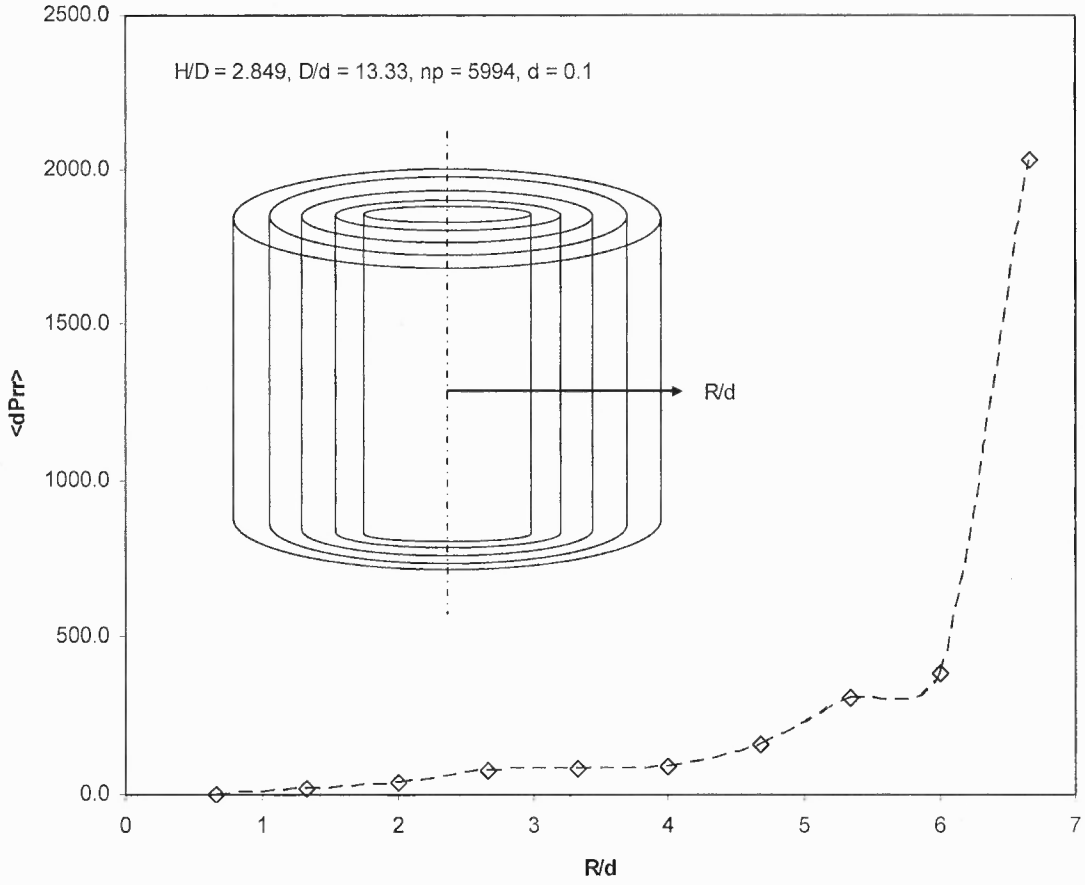

Figure 4.14 Differential average radial pressure in vertical layers of the cylinder. The lower regions of the R/d are close to the center of the cylinder and the upper regions of the R/d are close to the wall of the cylinder.

Figures 4.15 and 4.16 show the results for average radial pressure in vertical cross section layers with different radius particle diameter ratio versus time. The results for average radial pressure in these vertical cross section layers shows similar features with the horizontal cross section layers. However, the average radial pressure in vertical cross section layers has better consistency in results in comparison with the horizontal cross section layers; in addition there are fewer fluctuations in average radial pressure. The difference between the vertical and horizontal cross section layers is mostly due to the

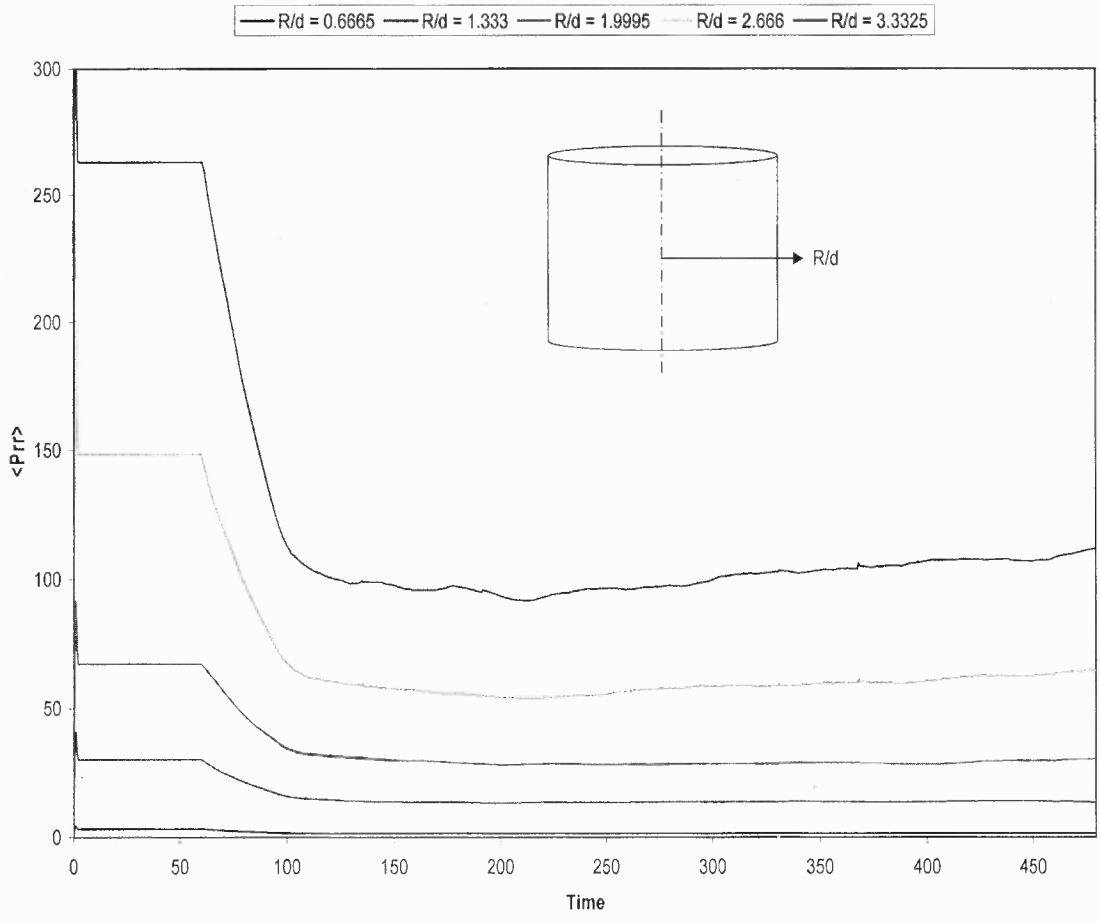

Figure 4.15 Average radial pressure in vertical cross section layers with the radius particle diameter ratio ranging from 0.6665 to 3.3325.

way in which the average radial pressure is being calculated. Since the entire fill height is used, there is more consistency in the average radial pressure. From the above analysis, the average radial pressure, <*Prr*>, is very unpredictable due to the particle configuration dependence.

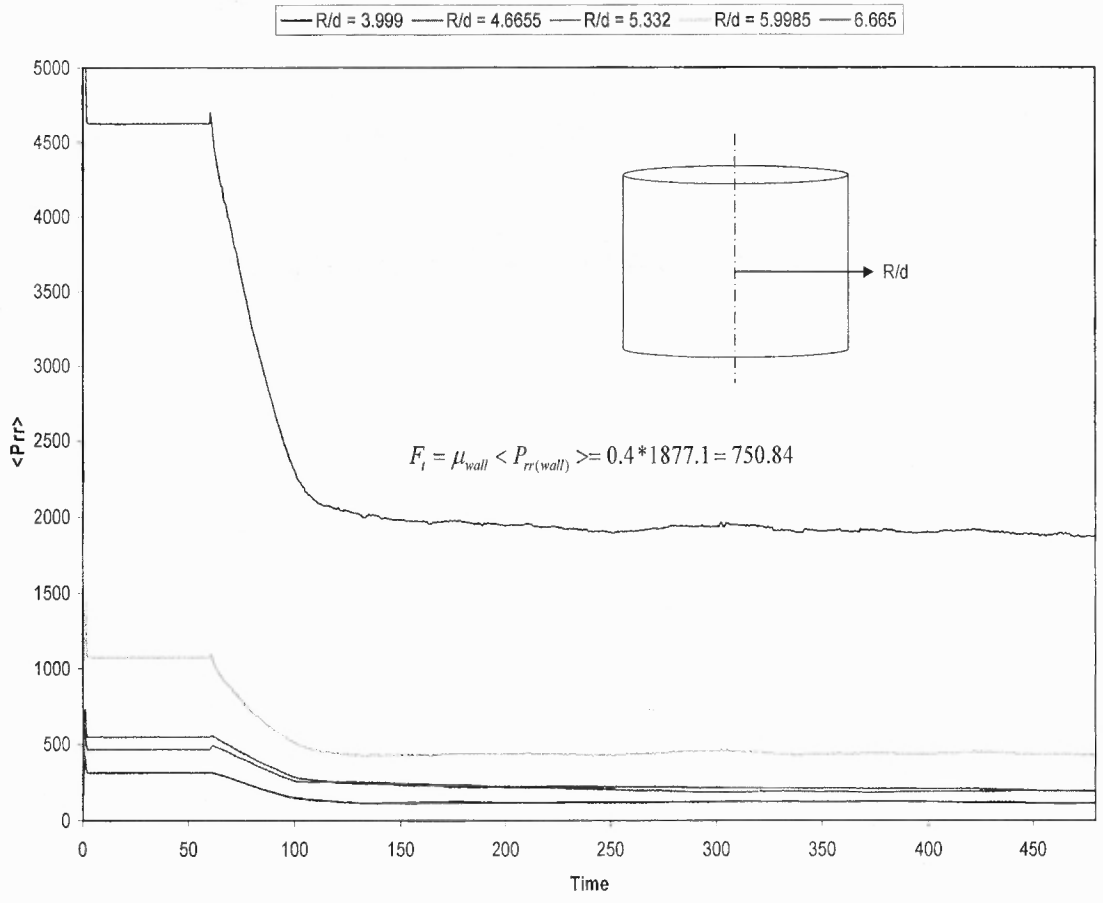

Figure 4.16 Average radial pressure in vertical cross section layers with the radius particle diameter ratio ranging from 0.3999 to 6.665.

4.3 Comparison with Experiments from Literature

As discussed in section 1.3, Walton [27–29] presented an experimental result that indicates an exponential form of the normal force versus the fill height relationship. Chester [6] then used DEM simulation to perform computation similar to the experiments of Walton. However, since the computing power was limited at the time, the work has been continued and expended in this thesis.

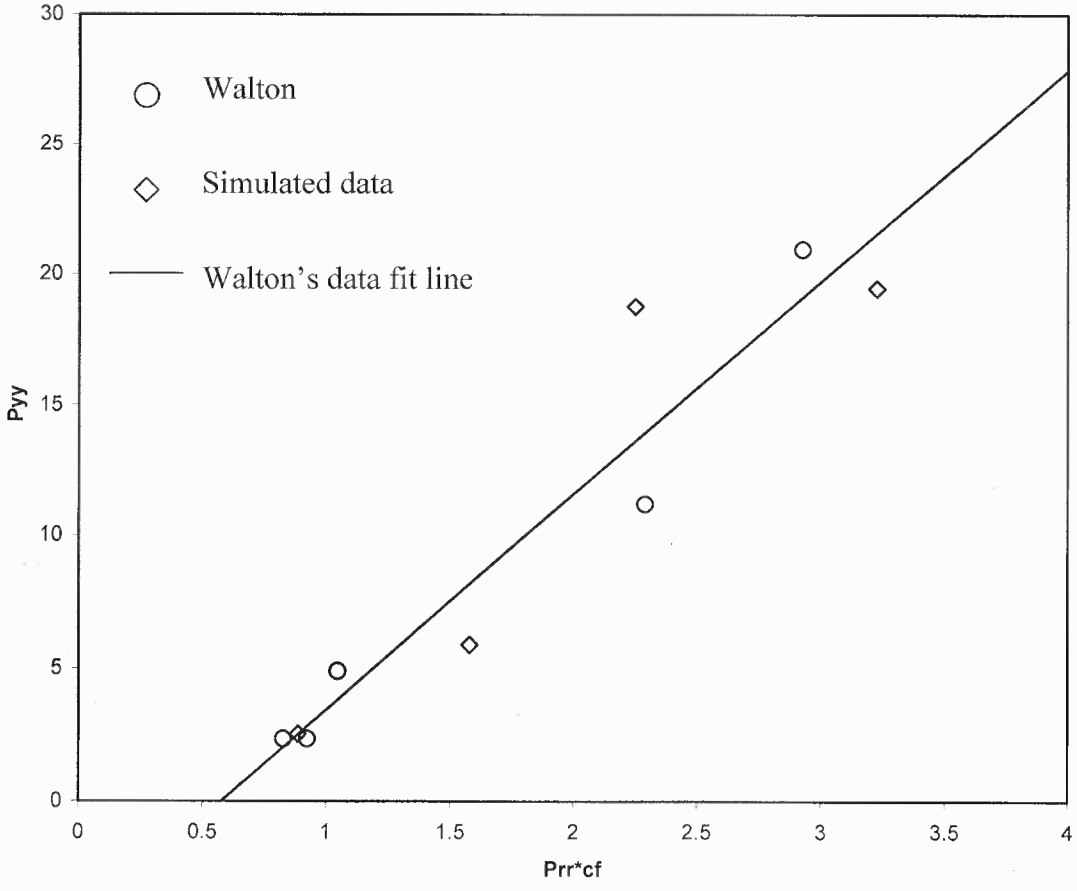

Figure 4.17 In comparison of the normal pressure versus average radial pressure (times the coefficient friction) between simulated data and Walton's experimental data [27].

Figure 4.17 shows the normal pressure versus the average radial pressure times the coefficient friction as Walton's published experimental data showed [27]. Walton's experiments were performed with 3 mm glass beads in a 4 cm acrylic tube. The diameter ratio used in this experiment was 13.33. The DEM simulation used the same parameters that Walton used in the experiments. These cases were small systems compared to the cases in the previous section. However, Figure 4.17 does show a linear relationship between the normal pressure and the radial pressure.

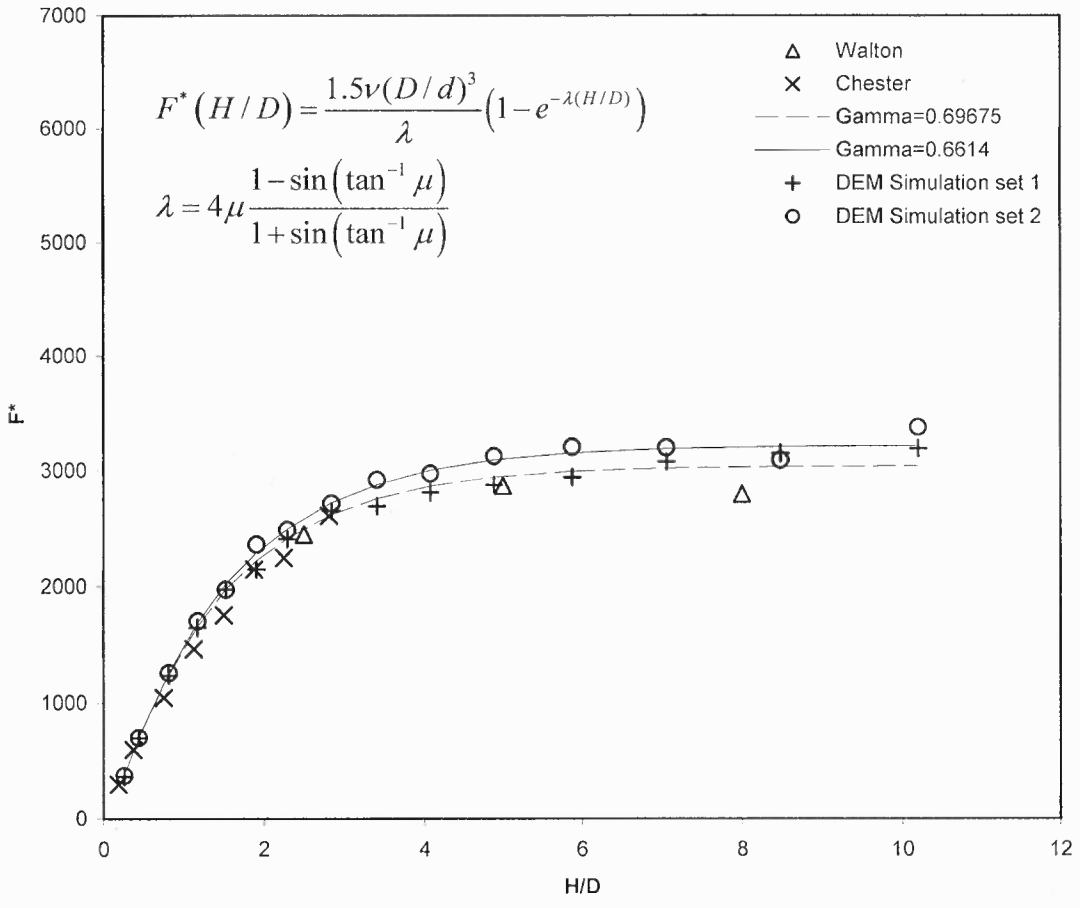

Figure 4.18 Comparison of simulated results to Walton's experimental results [13] and Chester's simulation results [6].

The triangles from Figure 4.18 are experiments from Walton. The (x) are the simulations from Chester's thesis. The black solid and dashed lines are, $\lambda = 0.69675$ and $\lambda = 0.6614$, the fit of the simulated results data. The (+) and (o) are the simulated results from Cases 16 – 45. As the figure shows, it is easily observed that the simulation data shows agreement with the experimental data.

CHAPTER 5

CONCLUSIONS AND FURTHER WORK

5.1 Conclusions

Discrete element simulations were performed to measure radial pressure and piston load of a cylindrical vessel. The granular materials used in these simulations were monodisperse with frictional inelastic spheres. The cylinder was set to 13.33 particle diameters for these radial pressure and piston load computations, and the fill heights are range from 0.262 to 10.172. The wall friction coefficients used in these simulations were set from 0.12 to 0.8 and the inter-particle friction coefficient set to 0.1 for all of the cases.

The radial void fraction calculation was performed in order to evaluate radial pressure in the cylinder. The parameters that were used in the first set of these simulations are to compare the experimental data [22]. The other set of the simulations parameters were taken from published Monte Carlo simulations [20]. The radial void fraction clearly shows the packing near the wall has a local region of order and this ordering effect becomes less prominent near the center of the cylinder. In addition, the ordering effect also can be seen at the bottom piston and this base effect is dependent on the fill height [21]. The simulated radial void fraction results show the packing algorithm can accurately simulate the static equilibrium positions for the loose packing of packed beds.

Static simulations were performed in which the wall friction was not activated. This was done by using a stationary piston at the bottom of the cylinder. The simulated average radial pressure and piston load versus fill height was found to have hydrostatic

behavior. The behavior for the static results was expected; where the fill heights increases, the radial pressure and piston load increases [6]. In addition, the simulation results show that the radial pressure was smaller than in dynamic simulations that were done in this thesis as well. This phenomenon was due to the fact that the wall friction was not activated, and therefore the radial pressures were only from inner-particle contacts.

Dynamic simulations were performed in which the wall friction was activated by translating the piston on the cylinder floor downwards with relatively small velocity. The simulation results show that the average radial pressure takes longer to reach equilibrium than the normal pressure at the bottom of the piston. The different in time between the radial pressure and the normal pressure depends on the height of the packed bed. In addition, the average radial pressure is strongly dependent on the packing configuration of the system. This dependence was found by calculating the average radial pressure in cross section layers of the cylinder. The results show that at the bottom of the pack, the average radial pressure shows small fluctuations. However, this fluctuation becomes more prominent as the cross section layers are close to the top of the cylinder. It is conjectured that the observed fluctuation behavior of the average radial pressure as the floor translates is a manifestation of the creation and destruction of force chains that have been reported in the literature [4, 19].

In addition to the dynamic simulations, the simulated average radial pressure shows that the particle-particle contact has less force then the particle-wall contact and has been investigated by Landry et al [16]. We show that as the fill height increases, the wall friction supports a greater fraction of the system weight in contrast to the normal

pressure. Furthermore, this ability to support the system weight grows with increasing the wall coefficient friction.

The dynamic simulated piston load agreed closely with the functional form of Janssen's theory for the diameter ratios. The simulation results show, as the fill height increases, the piston load becomes equilibrated and compares well with physical experiments and simulation results reported in the literature [6, 27]. The equilibrated region was caused by the friction coefficient of the wall. Moreover, as the wall coefficient friction increases, the piston load becomes equilibrated sooner because a greater weight of the particles is being supported by the wall friction as the fill height increases. In addition, the normal pressure on the piston versus average radial pressure graph shows a hydrostatic behavior in lower fill heights, but as fill heights increases, the linearity disappeared. This is because, there are fewer particles in the lower region of fill heights thus preventing the wall friction from taking full effect. As the fill heights increases, the wall friction takes effect and the average radial pressure increases as the normal pressure equilibrated.

The study of the radial pressure and the normal pressure violates Janssen's assumption that the lateral stress is a fixed fraction of the axial stress. Additionally, the pressure distribution across a horizontal layer is not uniform in a granular assembly as shown in these results.

5.2 Further Work

The work of this thesis provides a guideline for further work to better understand granular science. The list below shows some suggestions for further work.

A. Investigate cross section and radial layers of the cylinder vessel with a bigger system. The investigation should focus on the fluctuations in the system and the effect of fill height to these fluctuations.

B. Place a mass (or a mass particle) on top of the pack and see the effect of the radial pressure. Then increase the weight of the mass and see the associated changes to the radial pressure.

C. Investigate the force chain of the system and relate the work to the fluctuations in the average radial pressure.

D. Analyze the average radial pressure with higher floor velocities and understand the relationship between the floor velocity and radial pressure of the system.

APPENDIX A

MODIFICATIONS TO THE DEM CODE

This appendix details changes to the DEM code that for this thesis. Changes are described in an order of: a. which subroutine, b. where did modification take place and c. the modified code.

Main Program *3dshear.f*
The following lines of code initialized some of the parameters used in the simulation.

```
pi     = 3.141592653589798
ccpack = 0.7404804
half   = 0.5
third  = 0.33333333333
fourth = 0.25
fifth  = 0.2
sixth  = 0.166666666667
twith  = 0.05
tenth  = 0.1
one    = 1.0
two    = 2.0
three  = 3.0
four   = 4.0
ten    = 10.0
trifle = 1.0D-10
huge   = 1.0D+10
mt1 =1
is0 = 0
ircg = 0
```

Main Program *3dshear.f*
The following lines of code open the new output files in the simulation.

```
open(43,file='zradvol',status ='unknown')
open(45,file='zprrp',status='unknown')
open(46,file='zflprrp',status='unknown')
open(47,file='zdata',status='unknown')
```

Main Program *3dshear.f*
The following lines of code added to run the new subroutine *radfrac.f.*

```
c-----calculate interparticle for rzone
      if(t.gt.tout+dtout-half*dt) then
c     write(45,*)t
        call radfrac
      endif
c
```

Subroutine *datasav2.f*
The following lines of code print out the results for average radial pressure.

```
c-- modification by Meng Cui to print the stress
c     write(46,5001)t,cprrp,cflprrp
      do 800 n=1,nrzone
      do 801 m=1,nyzone
        write(45,5000) n,m,anprrp(n,m),danprrp(n,m)
 5000 format(i3,i3,1x,2e12.4,1x,2e12.4)
 5001 format(2(2e12.4))
 801  continue
 800  continue
```

Subroutine *diagnos2.f*
The following lines of code calculate the radial pressure.

```
c
      do 180 n=1,nrzone
      do 181 m=1,nyzone
         anprrp(n,m) = anprrp(n,m) + ABS(danprrp(n,m)*vorzoni(n,m))
         flprrp(n,m) = flprrp(n,m) + dflprrp(n,m)*voyzoni(m)
c
         cprrp = cprrp + danprrp(n,m)*vorzoni(n,m)
         cflprrp = cflprrp + dflprrp(n,m)*voyzoni(m)
c
 181  continue
 180  continue
c
```

Subroutine *forces.f*
The following lines of code calculate the radial pressure under force subroutine.

```
c
         do 28 n=1,nrzone
            do 29 m=1,nyzone
c
          if((vfrac(n,m,i).eq.0.0).and.(rrfr.eq.0.0)) then
            goto 29
          endif
c
            danprrp(n,m) = danprrp(n,m) + vfrac(n,m,i)*rrfr
            dflprrp(n,m) = dflprrp(n,m) + vfrac(n,m,i)*rnfn(5)
c
          if(danprrp(n,m).eq.NAN) then
c            write(43,*)rrfr,radialforce,raddistij
c          endif
c
 29         continue
 28       continue
C
```

APPENDIX B

VOLFRAC.F SUBROUTINE

In this appendix, subroutine volfrac.f is used in the FORTRAN code to compute the control volume of the sphere particle.

```
c%%%%%%%%%%%%%%%%%%%%%%%%%%%%%%%%%%%%%%%%%%%%%%%%%%%%%%%%%%%%%%%%%%%%%%%%%%%%
c subroutine radfrac.f will calculate the volume fraction of a sphere
c inside
c an annular layer created Oct.22 2007 by Meng Cui
c updated on Jan. 31 2008
c
      subroutine radfrac
      include 's3dscmm'
      integer*4 iter
      real*8 area,cellvol(mp),dal,dah,deltar,deltay
      real*8 p,r,rady,rp,rstart,rstop,rvol(mp),radsol
      real*8 ybot,ytop,ymax,ylocation,yvol
      real*8 radialvol(mp),totv(mp),totalvol,volcylinder
      real*8 solidfrac
c
c%%%%%%%%%%%%%%%%%%%%%%%%%%%%%%%%%%%%%%%%%%%%%%%%%%%%%%%%%%%%%%%%%%%%%%%%%%%%
c
c------setup numbers of intervals
      iter=1500
c
c------Calculate maxium height of the particles in the cylinder
      ymax = y(1)
      do 100 h=ind1,ind2
         if(y(h).gt.ymax) then
         ymax = y(h)
       endif
 100  continue
      ymax = ymax + radius(1)
c
      totalvol = 0.0
      solidfrac = 0.0
c
      do 101 n=1,nrzone
         rvol(n) = 0.0
         cellvol(n) = 0.0
 101  continue
c
c------Calculate the maxium volume of the cylinder
c------This is not the real volume of the cylinder
c------Only use this for solid fraction calculations
      volcylinder = pi*(radius(3)*radius(3))*ymax
c
c------Loop the particles
      do 1 i=ind1,ind2
c
c------calculate the total volume of the particle
```

```
      totv(i) = 4.*third*pi*rad(i)*rad(i)*rad(i)
c
c------calculate the distance between a particle and the cylinder
         rp=sqrt(x(i)*x(i)+z(i)*z(i))
c
c------Setup r-zone
         do 2 n=1,nrzone
            rstart = (n-1)*drzone
            rstop = n*drzone
c
c------Calculate cell volume
            cellvol(n) = pi*((rstop*rstop)-(rstart*rstart))*ymax
c
c------Setup y-zone
            do 3 m=1,nyzone
               ybot = (m-1)*dyzone
               ytop = m*dyzone
c
c------setup intervals in r-y-zone
               deltar = (rstop-rstart)/iter
               deltay = (ytop-ybot)/iter
c
c------initalize the radialvol(i)
               radialvol(i) = 0.0
             vorzoni(n,m)=pi*((rstop*rstop)-(rstart*rstart))*ymax
c
c------loop the intervals in y-zone
               do 4 j=1,iter
                  ylocation=ybot+((j-1)*deltay)
                  if(abs(ylocation-y(i)).ge.rad(i)) then
                     goto 4
                  endif
                  rady=sqrt((rad(i)*rad(i))-((ylocation-y(i))
     1                 *(ylocation-y(i))))
c
c------initalize the area
                  area = 0.0
c
c------loop the intervals in r-zone
               do 5 k=1,iter
                  r = rstart + (k*deltar)
c
c------CASE 1
               if((r+rady).le.rp) then
                  goto 5
c------CASE 2
               elseif((r.gt.rady).and.((r-rady).ge.rp)) then
                  goto 5
c------CASE 3
               elseif((r.lt.rady).and.((rady-r).ge.rp)) then
                p = 2*pi*r
c------CASE 4
               else
                  dal = (r*r-rady*rady+rp*rp) / (2*rp)
                  dah = sqrt(r*r-dal*dal)
                  theta = 2*(ATAN(dah/dal))
                  p = theta*r
```

```
                endif
c
c------calculate the area of this section
              area = area + p*deltar
c
 5              continue
c
c------calculate volume of the section
                radialvol(i) = radialvol(i) + area*deltay
c
 4              continue
c
c------Calculation of volume fraction
              vfrac(n,m,i) = radialvol(i) / totv(i)
c
c------Calculate volume in the entire r-zone
                rvol(n) = rvol(n) + radialvol(i)
c
 3              continue
c
c------Calculate the volume in the entire y-cell
                yvol = yvol + rvol(n)
c
 2              continue
c
c------The volume of the entire cylinder
                totalvol = totalvol + yvol
c
 1              continue
c------Solid Fraction for the entire cylinder
c------Not very useful
                solidfrac = totalvol/volcylinder
c
                do 3000 n=1,nrzone
                   radsolid = rvol(n)/cellvol(n)
                   write(43,500)n,t,radsolid,ymax
 3000           continue
c
 500       format(i3,2(1x,4e12.4))
c
                end
```

REFERENCES

1. A. Wouterse, and A.P. Philipse, *Geometrical Cluster Ensemble Analysis of Random Sphere Packings.* The Journal of Chemical Physics, 2006. **125**(194709).

2. O.R. Walton and R.L. Braun, *Viscosity and Temperature Calculations for Assemblies of Inelastic, Frictional Disks.* Journal of Rheology, 1986. pp.949-980.

3. O.R. Walton and R.L. Braun, *Stress Calculations for Assemblies of Inelastic Spheres in Uniform Shear.* Acta Mechanica, 1986. **63**, pp.73-86.

4. B. Tighe, J. Socolar and D. Schaeffer, *Force Chain Networks and the Stress Response of Granular Materials.* XXI ICTAM, August 2004. pp.15-21.

5. C.R.A. Abreu, R. Macias-Salinas, F.W. Tavares and M. Castier, *A Monte Carlo Simulation of the Packing and Segregation of Spheres in Cylinders.* Braz. J. Chem. Eng., Dec. 1999. **16**. n.4

6. S.A. Chester, *DEM Simulated Floor Pressure Induced by a Granular Column.* Master's Thesis, New Jersey Institute of Technology. 2006.

7. P.A. Cundall and O.D. Strack, *A Discrete Numerical Model for Granular Assemblies.* Geotechnique. 1979. **21**. pp.47-65.

8. W. Goldsmith, *Impact*, E. Arnold Publishers, 1990.

9. S.P. Timoshenko and J.N. Goodier, *Theory of Elasticity*, 3rd edition, pg. 412, McGraw Hill, 1970.

10. J. Theuerkauf and D. Schwesig, *Analysis of Particle Porosity Distribution in Fixed Beds Using the Discrete Element Method.* Powder Technology, 2006. **165**. pp.92-99.

11. H.A. Janssen. *Versuche über Getreidedruck in Silozellen*, Zeitschr. d. Vereines deutscher Ingenieure, **39**(35):1045-1049, 1895.

12. H.J. Kim, *Particle Dynamics Modeling of Boundary Effects in Granular Couette Flow.* Ph. D. Dissertation, New Jersey Institute of Technology, 1992.

13. L.F. Liu, Z.P. Zhang and A.B. Yu, *Dynamic Simulation of the Centripetal Packing of Mono-Sized Spheres.* Physica A, 1999. **268**. pp.433-453.

14. F. Lamarche and C. Leroy, *Evaluation of the Volume of Intersection of Sphere with A Cylinder by Elliptic Integrals.* Computer Physics Communications, 1990. **59**. pp.359-369.

15. Y. Lan, *Particle Dynamics Modeling of Vibrating Granular Beds.* Ph. D. Dissertation, New Jersey Institute of Technology, 1994.

16. J.W. Landry, *Confined Granular Packings: Structure, Stress and Forces.* Physical Review E, 2003. **67**(041303).

17. J.W. Landry and G.S. Grest, *Granular Packings with Moving Side Walls.* Physical Review E, 2004. **69**(031303).

18. S. Luding, *Models and Simulations of Granular Materials, in Theoretische polymerphysik.* 1994, Albert-Ludwigs-Universitat: Freiburg. pp. 125-453.

19. M.E. Cates, J.P. Wittmer, J.P. Bouchanud, and P. Claudin, *Jamming, Force Chains, and Fragile Matter.* Physical Review Letters, 1998. **81**. pp.1841-1844.

20. G.E. Mueller, *Radial Void Fraction Distributions in Randomly Packed Fixed Beds of Uniformly Sized Spheres in Cylindrical Containers.* Powder Technology, 1991. **72**. pp.269-275.

21. G.E. Mueller, *Numerical Simulation of Packed Beds with Monosized Spheres in Cylindrical Containers.* Powder Technology, 1997. **92**. pp.179-183.

22. G.E. Mueller, *Numerically Packing Spheres in Cylinders.* Powder Technology, 2005. **159**. pp.105-110.

23. R.M. Nedderman, *Statics and Kinematics of Granular Materials.* 1992, Cambridge, U.K.:Cambridge University Press. 352.

24. N.J.A. Sloane, *The On-Line Encyclopedia of Integer Sequences.* Sequence A133741, 1999.

25. I.A. Stegun and M. Abramowitz *Handbook of Mathematical Functions*. 1965, Dover Publications.

26. M. Sweetman, *Addition of a Chain-Cell Method and a Van der Waals Force Model to a Particle Dynamics code.* Ph. D. Dissertation, New Jersey Institute of Technology, 2003.

27. O.R. Walton, *Numerical Simulation of Inclined Chute Flows of Monodisperse, Inelastic, Frictional Spheres. In Second U.S.-Japan Seminar on Micromechanics of Granular Materials.* 1991. Potsdam, NY:Elsevier.

28. O.R. Walton, "*Force Models for Particle-Dynamics Simulations of Granular Materials*", in Mobile Particulate Systems, ed. E.Guazzell & L. Oger, NATO AS1 Series E: Applied Sciences, Vol. 287, Kluwer Academic Publishers, Ch.20, pg. 367, 1995.

29. O.R. Walton, *Potential Discrete Element Simulation Applications Ranging From Airborne Fines to Pellet Beds.* SAE 2004 Transactions: J. Aerospace, 2004. 2004-01-2329: pp.1-14.